AD_____

Award Number: W81XWH-06-1-0071

TITLE: Predicting Bone Metastatic Potential of Prostate Cancer via Computational Modeling of TGF-β Signaling

PRINCIPAL INVESTIGATOR: Carlton R. Cooper
Babatunde Ogunnaike

CONTRACTING ORGANIZATION: University of Delaware
Newark, DE 19716

REPORT DATE: May 2008

TYPE OF REPORT: Final

PREPARED FOR: U.S. Army Medical Research and Materiel Command
Fort Detrick, Maryland 21702-5012

REPORT DOCUMENTATION PAGE

Form Approved
OMB No. 0704-0188

1. REPORT DATE *(DD-MM-YYYY)*	**2. REPORT TYPE**	**3. DATES COVERED** *(From - To)*
01-05-2008	Final	30 OCT 2005 - 29 APR 2008

4. TITLE AND SUBTITLE

Predicting Bone Metastatic Potential of Prostate Cancer via Computational Modeling of TGF-β Signaling

5a. CONTRACT NUMBER

5b. GRANT NUMBER
W81XWH-06-1-0071

5c. PROGRAM ELEMENT NUMBER

6. AUTHOR(S)
Carlton R. Cooper; Babatunde Ogunnaike

E-Mail: crcooper@udel.edu

5d. PROJECT NUMBER

5e. TASK NUMBER

5f. WORK UNIT NUMBER

7. PERFORMING ORGANIZATION NAME(S) AND ADDRESS(ES)

University of Delaware
Newark, DE 19716

8. PERFORMING ORGANIZATION REPORT NUMBER

9. SPONSORING / MONITORING AGENCY NAME(S) AND ADDRESS(ES)
U.S. Army Medical Research and Materiel Command
Fort Detrick, Maryland 21702-5012

10. SPONSOR/MONITOR'S ACRONYM(S)

11. SPONSOR/MONITOR'S REPORT NUMBER(S)

12. DISTRIBUTION / AVAILABILITY STATEMENT
Approved for Public Release; Distribution Unlimited

13. SUPPLEMENTARY NOTES

14. ABSTRACT
This hypothesis generation project involved the development of a computational model of the TGF-β signaling pathway and investigating whether such a model can be used to generate hypotheses regarding metastatic potential of prostate cancer (PCa). The primary "deliverable" of the investigation is a comprehensive quantitative model of TGF-β signaling that is representative of a wide variety of experimental data collected in different labs worldwide; the primary outcome is the following set of related conclusions: (i) it is possible to use such a model to predict metastatic potential of PCa,; but (ii) to do so appropriately requires a deeper quantitative understanding of the role of TGF-β as a regulator of prostate gland function; and in this regard, (iii) that the primary role of TGF-β as a tumor suppressor may still be intact so that the observed over-expression in poor prognosis PCa patients is due to changes in the PCa cells and not in the ligand.

15. SUBJECT TERMS
Transforming growth factor signaling, computer modeling, prostate cancer metastasis

16. SECURITY CLASSIFICATION OF:			**17. LIMITATION OF ABSTRACT**	**18. NUMBER OF PAGES**	**19a. NAME OF RESPONSIBLE PERSON**
a. REPORT	**b. ABSTRACT**	**c. THIS PAGE**			USAMRMC
U	U	U	UU	55	**19b. TELEPHONE NUMBER** *(include area code)*

Standard Form 298 (Rev. 8-98)
Prescribed by ANSI Std. Z39.18

TABLE OF CONTENTS

PREDICTING BONE METASTATIC POTENTIAL OF PROSTATE CANCER VIA COMPUTATIONAL MODELING OF TGF-β SIGNALING

PI: *Carlton R. Cooper,* ***Co-PI:*** *Babatunde A. Ogunnaike 10/05 – 5/07; No-cost extension granted to 5/08*

INTRODUCTIONS

The TGF-β1 family is part of a collection of cytokines responsible for controlling a wide range of cellular processes involved with growth and proliferation [1]. In particular, TGF-β1 is generally known as a potent inhibitor of proliferation in normal epithelial cells. However, in cancer cells, it is also known to induce cellular dynamics necessary for metastasis; and its level is elevated in patients with prostate cancer, raising some fundamental questions [5, 4, 3, 2]: (i) how can a single stimulus produce multiple contradictory results in different cell types; and (ii) can an understanding of this phenomenon be harnessed for more precise prediction of metastatic potential of prostate cancer? From currently available information in the literature, the role of TGF-β on prostate cancer development and metastasis is clearly too complex for a qualitative description to be useful in answering these questions: to understand the various, and sometimes contradictory, effects of TGF-β on prostate cancer cells, true quantitative insight that will enable predictive understanding requires mathematical modeling of the phenomena of TGF-β signaling in normal and cancerous cells

BODY

This ***hypothesis generation*** project involved the development of a computational model of the TGF-β signaling pathway and investigating whether such a model can be used to generate hypotheses regarding metastatic potential of PCa. We now have a comprehensive quantitative model of TGF-β signaling that is representative of a wide variety of experimental data collected in different labs worldwide. The primary outcome of the project is the following set of related conclusions: (i) it is possible to use such a model to predict metastatic potential of PCa; but (ii) to do so appropriately requires a deeper quantitative understanding of the role of TGF-β as a regulator of prostate gland function; and in this regard, (iii) that the primary role of TGF-β as a tumor suppressor may still be intact so that the observed over-expression in poor prognosis PCa patients is due to changes in the PCa cells and not in the ligand.

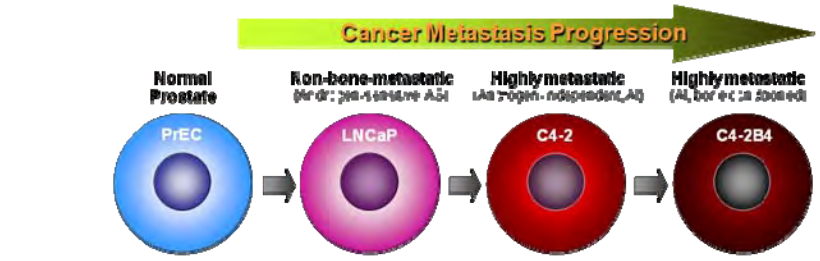

Growth	Normal	No change	Dose-dependent inhibition	DD inhibition
Adhesion	-	Increase	Decrease	Decrease
TβRII	Normal	Low	Low	High
TβRI	Normal	Low	Low	High
TβRII mRNA	Normal	Present	Present	Present
Smad2	Normal	?	?	?
Smad4	Normal	?	?	?
p-Smad2	Normal	High	High	?

Fig 1. Proposed PCa cell model plan and experimental conditions to be investigated.

A full account of the model development and results is

contained in Chung et al, 2008, (submitted for publication.) This project has enabled us to generate hypotheses and ideas that we are currently exploring in an "Idea Generation Proposal" recently submitted to the DoD. In this newly proposed work, we will extend the model to represent specific stages of PCa progression as illustrated in (**Fig. 1)** in addressing point (ii) above, and then develop a control-system model of TGF-β1-mediated regulation of the prostate gland regulation to investigate the idea expressed in point (iii) above about the role of TGF-β1 as a tumor suppressor in both normal and PCa cells. Specifically, we will investigate the idea that as a result of a control system that employs TGF-β for prostate gland regulation, the observed increased level of TGF-β in poor prognosis PCa patients is a *consequence* of acquired TGF-β resistance in the prostate cancer cell, *not the cause*.

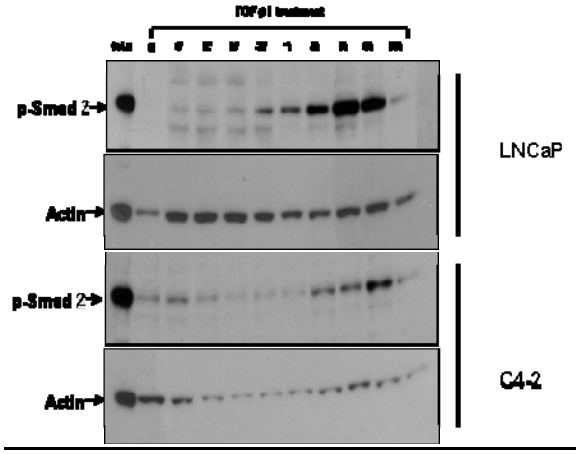

Fig 2. Western Blot of Smad 2 phosphorylation: LNCaP and C4-2 were treated with 10ng/ml of TGF-β1 with protein isolated at specific time intervals and probed for Smad 2 phosphorylation. Actin is used as a loading control.

The key results of the experimental component of the project are as follows: the biological data we collected demonstrate that as a non-metastatic cell line (LNCaP) progresses to a more aggressive cell line (C4-2B4), adhesion to bone-marrow endothelial cells (BMEC) decreases in response to TGF-β1; there is also an increase in the ability of TGF-β1 to inhibit prostate cancer growth, and an increase in TRII and TRI expression. Further, our experiments also demonstrated (**Fig 2**) that TGF-β1-mediated Smad2 activation was delayed and attenuated in the more aggressive C4-2 subline compared to LNCaP. TGF-β1 activated Smad2 within 30 minutes in LNCaP, but 2 hours were required to activate Smad2 in C4-2. Further, the level of Smad2 activation was higher in LNCaP compared to C4-2. In support of attenuated TGF-β1 signaling, C4-2 was more resistant to TGF-β1 growth suppression compared to LNCaP (Fig 3). Bone marrow derived C4-2B4 and PC-3 cells are more sensitive to TGF-β1-induced growth suppression, which is surprising considering that the bone matrix is a repository for TGF- β1. Some of these results were presented at the 2007 IMPaCT conference.

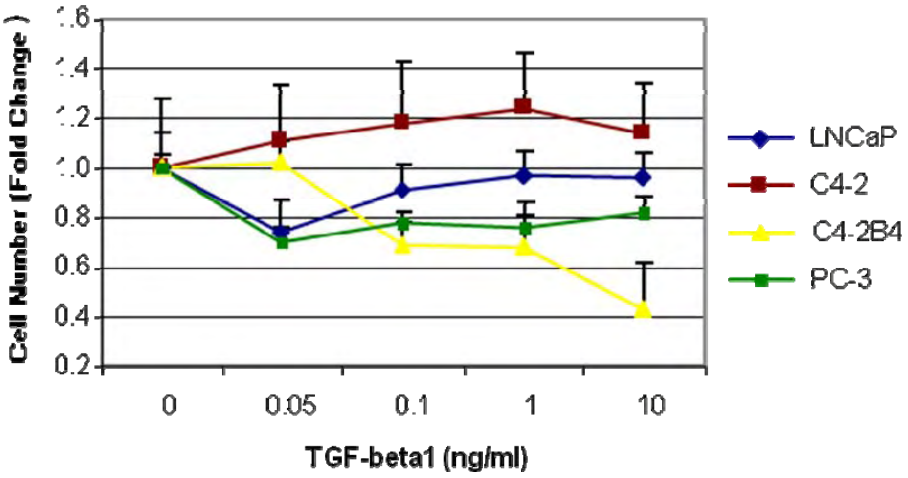

Fig 3. The effect of TGF-β1 on the growth of PC cells with varying metastatic potential.

During the award period, the participating graduate students, Ms. Fayth Miles in the Biological Sciences Dept., and Mr. Seung-Wook Chung in the Chemical Engineering Dept. respectively published a paper, and successfully defended a Master's thesis on the work done on this project. They are both continuing work on their respective PhD dissertations. A joint paper (Chung et al, 2008) has been submitted for publication in the Biophysical Journal; a copy of the manuscript is attached.

KEY ACCOMPLISHMENTS

The major accomplishments are as follows:

1. Experimentally, we demonstrated differential TGF-β1 signaling in prostate cancer cells with varying metastatic abilities;

2. We also demonstrated that differential TGF- β1 signaling in prostate cancer cells correlate to their sensitivity to TGF- β1 mediated growth suppression;

3. We have developed a quantitative model of the TGF- β1 signaling pathway and used it to generate several hypotheses that we plan to investigate in a recently submitted Idea proposal (see attached abstract).

REPORTABLE OUTCOMES

See attached Manuscript and review article in the appendices

CONCLUSIONS

A computational model of the TGF-β signaling pathway (supported by experimental data) can in fact be used to generate hypotheses regarding metastatic potential of PCa, but this requires a deeper quantitative understanding of the role of TGF-β as a regulator of prostate gland function. In this regard, this hypothesis exploration study has led directly to the generation of the hypothesis that the observed increased level of TGF-β in poor prognosis PCa patients is a *consequence* of acquired TGF-β resistance in the prostate cancer cell, *not the cause*. We plan to explore and test this hypothesis in a recently submitted "Idea Generation" proposal entitled "A computational modeling approach to elucidating the complex role of TGF-β in prostate cancer progression"

REFERENCES

1. **Akhurst, R.J., and Derynck, R. (2001). TGF-beta signaling in cancer--a double-edged sword. Trends Cell Biol 11, S44-51.**

2. **Miles, F.L., Pruitt, F.L., van Golen, K.L., and Cooper, C.R. (2008). Stepping out of the flow: capillary extravasation in cancer metastasis. Clin Exp Metastasis 25, 305-324.**

3. **Tu, W.H., Thomas, T.Z., Masumori, N., Bhowmick, N.A., Gorska, A.E., Shyr, Y., Kasper, S., Case, T., Roberts, R.L., Shappell, S.B., Moses, H.L., and Matusik, R.J. (2003). The loss of TGF-beta signaling promotes prostate cancer metastasis. Neoplasia 5, 267-277.**

4. **Wikstrom, P., Damber, J., and Bergh, A. (2001). Role of transforming growth factor-beta1 in prostate cancer. Microsc Res Tech 52, 411-419.**

5. **Wikstrom, P., Stattin, P., Franck-Lissbrant, I., Damber, J.E., and Bergh, A. (1998). Transforming growth factor beta1 is associated with angiogenesis, metastasis, and poor clinical outcome in prostate cancer. Prostate 37, 19-29.**

Appendices

Quantifying the Role of TGF-β1 in Prostate Cancer Metastasis: Computer Modeling and Experimental Studies

Fayth L. Miles, Seung-Wook Chung, Robert A. Sikes, Babatunde Ogunnaike and Carlton Cooper

TGF-β1 is generally known as a potent inhibitor of proliferation in normal epithelial cells. However, in cancer cells, it is also known to induce cellular dynamics necessary for metastasis; and its level is elevated in patients with prostate cancer, raising some fundamental questions: (i) how can a single stimulus produce multiple contradictory results in different cell types; and (ii) can an understanding of this phenomenon be harnessed for more precise prediction of metastatic potential of prostate cancer? From currently available information in the literature, the role of TGF-β on prostate cancer development and metastasis is clearly too complex for a qualitative description to be useful in answering these questions: to understand the various, and sometimes contradictory, effects of TGF-β on prostate cancer cells, true quantitative insight that will enable predictive understanding requires mathematical modeling of the phenomena of TGF-β signaling (and transcriptional regulation) in normal and cancerous cells.

We have used the LNCaP Progression Model of increasingly metastatic lineage-related prostate cancer cells to study the effects of TGF-β1 on metastasis and to construct a dynamic mathematical model used to quantify TGF-β1-stimulated bone-metastatic potential of prostate cancer cells at different stages in metastasis (Fig. 1). The experimental results show, among other things, that at the cell population level, TGF-β1 appears to regulate growth as well as adhesion to bone marrow endothelium differentially in nonmetastatic and metastatic PCa cells; growth is inhibited in C4-2 and C4-2B4 cells but not in LNCaP; there is a decrease in the TGF-β1-induced adhesion of C4-2 and C4-2B4 to BMEC; and there is no change in PCa adhesion to TGF-β1-treated BMEC, suggesting that the changes in adhesion are the result of activation of TGF-β1 signaling in the PCa cells, and not BMEC. In addition, western blot data show that the classic TGF-β1 Type II receptor is expressed at similar, albeit low levels in LNCaP and C4-2 cells, and higher levels in the bone-derived C4-2B4 cells. Additional results show that Smad 2, one of the main effectors in the pathway, is activated in both LNCaP and C4-2, with earlier and more robust activation in LNCaP.

While it is evident that all the cell lines have active TGF-β1 signaling pathways, the detailed mechanism of how TGF-β1 induces different responses via signaling effectors during cancer progression remains poorly understood. To identify and quantify the role of TGF-β1 in cancer metastasis, we have developed a dynamic mathematical model of the TGF-β1 signaling pathway for normal prostate epithelial cells (PrEC) and three prostate cancer cell lines, LNCaP, C4-2, and C4-2B4 (Figure 1). The model is used to analyze the characteristics of the pathway in terms of the dynamic behavior of the signaling effectors, and determine which steps are most critical and sensitive. *In silico* mutations, (simulations of discrete mutation events) are used to understand how variations in the TGF-β pathway during progression affect specific metastatic events such as adhesion and eventually migration. Overall, the information generated from this investigation could be useful for accurately predicting the metastatic potential of advanced localized prostate cancer and subsequently better select patients for more aggressive therapy.

Appendices

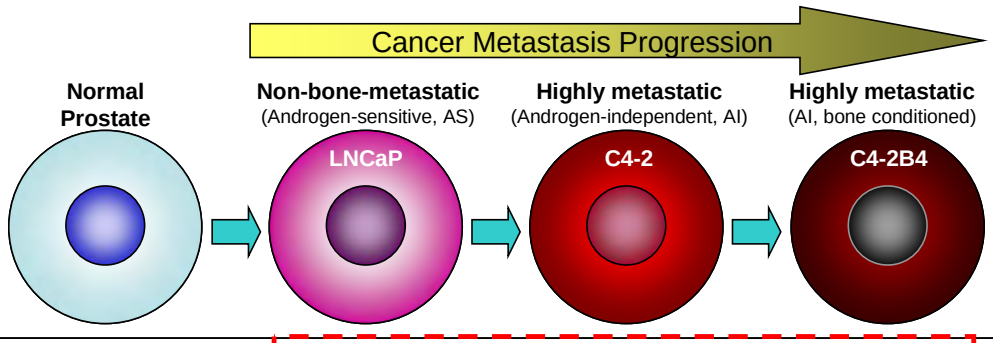

Growth	Normal		No change	Dose-dependent inhibition	DD inhibition
Adhesion	-		Increase	Decrease	Decrease
TβRII	Normal		Low	Low	High
TβRI	Normal	?	Low	Low	High
TβRII mRNA	Normal		Present	Present	Present
Smad2	Normal		?	?	?
Smad4	Normal		?	?	?
p-Smad2	Normal		High	High	?

Figure 1. *Discrete states in prostate cancer progression*

An Integrated Computational Model of The Transforming Growth Factor β (TGF-β) Signaling Pathway

Seung-Wook Chung[1], Fayth L. Miles[2],
Carlton R. Cooper[2], Mary C. Farach-Carson[2],
and Babatunde A. Ogunnaike[1§]

[1]Department of Chemical Engineering,
[2]Department of Biological Sciences,
and
Center for Translational Cancer Research
University of Delaware, Newark, Delaware 19716

§ To whom correspondence should be addressed: Babatunde A. Ogunnaike, William L. Friend Professor, Dept. of Chemical Engineering, University of Delaware, Newark, DE 19176. Tel.: 302-831-4504; Fax: 302-831-1048; E-mail: ogunnaike@UDel.Edu

ABSTRACT

Transforming growth factor β (TGF-β) signaling regulates a wide range of cellular and physiologic processes including proliferation, cell survival, differentiation, migration, angiogenesis, and immune surveillance. It therefore is not surprising that this ligand plays a significant role in the development and progression of cancer. The current consensus is that TGF-β affects tumor pathogenesis both positively and negatively, functioning as a tumor suppressor in the premalignant stages of tumorigenesis and as a tumor promoter in later stages of cancer leading to metastasis. Despite its prominent role in both normal and cancerous cellular processes, the detailed mechanisms of how TGF-β induces such diverse and sometimes contradictory responses remain poorly understood. As a first step in understanding TGF-β signaling quantitatively, we have developed a comprehensive, dynamic model of the canonical TGF-β pathway via Smad transcription factors (the major intracellular mediators of the signaling cascade), based on the most up-to-date information available in the literature. We fit the model simultaneously to several sets of experimental data from the literature and validated the predictions of the finalized model independently against a different collection of experimental data.

By describing how an extracellular signal of the TGF-β ligand is sensed by receptors and transmitted into the nucleus through intracellular Smad proteins, the model yields quantitative insight into how TGF-β-induced responses are modulated and regulated. Considering that Smad nuclear accumulation is necessary for transcriptional regulation, our model analysis reveals that mechanisms associated with Smad activation by ligand-activated receptor, nuclear complex formation among Smad proteins, and inactivation of ligand-activated Smad (e.g. degradation, dephosphorylation) may be critical for regulating TGF-β-targeted functional responses by affecting the intensity and duration of nuclear retention of Smad proteins. The model was also used to predict possible dynamic characteristics of the Smad-mediated pathway in abnormal cells, and to provide clues regarding possible mechanisms to explain the seemingly contradictory roles of TGF-β during cancer progression.

Based on reported observations that TGF-β receptors are abnormal in a variety of human cancers, our model simulations of cancerous cell signaling indicate that a reduction in the levels of functional receptors may lead to altered TGF-β signaling behavior where tumor suppression characteristics are lost as a result of attenuated and transient Smad nuclear accumulation. Considering the differences in the dynamics of transcriptionally active, nuclear-localized Smad between normal and cancerous signaling systems, the TGF-β paradox may be explained partially by the following postulated hypotheses: (1) signaling thresholds of anti-oncogenic responses are different from those of pro-oncogenic responses; (2) cancer utilizes mechanisms associated with rapid degradation of major signaling components in the pathway; and (3) tumor-suppressing effects mediated by Smad4 and tumor-promoting effects mediated by potential binding factors of pSmad2 are unbalanced during cancer progression.

INTRODUCTION

Transforming growth factor-β (TGF-β) proteins are members of a superfamily of secreted cytokines that control a diverse array of cellular processes including cell proliferation, differentiation, motility, adhesion, angiogenesis, apoptosis, and immune surveillance (1-3). The TGF-β signaling cascade begins when extracellular TGF-β binds to and brings together Type I and Type II TGF-β receptor serine/threonine kinases on the cell surface, whereby the Type II receptor phosphorylates and activates the Type I receptor. The activated Type I receptor, in turn, propagates the signal through phosphorylation of receptor-bound (R-)Smad transcription factors (Smad2/3 and Smad1/5/8) at the carboxy-terminal SXS motif. The activated R-Smads form hetero-oligomers with Smad4 as a common partner and rapidly translocate into the nucleus, undergoing continuous nucleocytoplasmic shuttling by interacting with the nuclear pore complex. Once in the nucleus, activated Smad complexes bind to specific promoters and ultimately regulate expression of target genes through interactions with other transcriptional co-activators and co-repressors, generating approximately five hundred gene responses in a cell- and context-specific manner (1, 2, 4-6).

The TGF-β signaling pathway has become an attractive but difficult target for oncology drug development because of its apparently paradoxical roles in tumorigenesis and metastasis. In normal and early phase tumorigenic epithelial cells, TGF-β functions as a potent tumor suppressor primarily by inducing cell cycle arrest and apoptosis. However, in the intermediate and late stages of carcinogenesis, tumor cells become resistant to the growth inhibitory effects of TGF-β and show elevated expression of TGF-β. The ligand is over-expressed in clinical cancer samples, with increasing levels correlating with poor clinical outcomes. The role of TGF-β therefore *appears* to become one of tumor promotion, apparently supporting growth, subverting the immune system, and also facilitating, invasion, epithelial to mesenchymal transition (EMT), and angiogenesis. This finding has created the widely held perception that TGF-β acts as a tumor *promoter* in advanced tumorigenesis and metastasis (7-9) . While it is known that most cancer cell lines representing the entire spectrum of tumor progression have active TGF-β signaling pathways, detailed mechanisms of how a single stimulus, TGF-β, induces such a diverse array of responses during cancer progression remains poorly understood. This is primarily due to the complexity of the signaling cascade system in which a variety of signaling components changing dynamically over different time scales interact with one another. Quantitative understanding and analysis of such a complex regulatory circuit are not possible via qualitative human intuition alone; quantitative descriptions that lead to predictive models are necessary, and have become useful in improving our understanding of this complex signaling pathway.

Although significant progress has been made in understanding the biochemistry of the TGF-β pathway, to the best of our knowledge, only five mathematical models of TGF- β signaling have been published, each focused on restricted portions, not the entire pathway (10-12). Vilar and coworkers (10) explored a model of TGF-β signal processing at the receptor level. They modeled TGF-β receptor trafficking events taking place concurrently at the plasma membrane and in endosomes, and they incorporated the processes of internalization into endosomes, recycling to the plasma membrane, constitutive and ligand-induced receptor degradation, and receptor protein synthesis. In contrast, Clarke *et al.* (11) focused on intracellular signaling via the Smad-mediated pathway, incorporating into both the cytoplasm and the nucleus several steps such as R-Smad phosphorylation and dephosphorylation, nucleocytoplasmic shuttling of Smad proteins. However, this model does not show a direct relationship between an

extracellular TGF-β ligand and intracellular responses because signaling is initiated by the activated receptor complex, not by TGF-β ligand itself. The dynamic behavior of the ligand-stimulated receptor complex was described by a simple decreasing exponential function.

The model presented by Melke and coworkers (12) for TGF-β signal transduction in endothelial cells included two Type I receptors (ALK1 for Smad1/5/8 and ALK5 for Smad2/3), simplified the ligand-receptor binding step by considering Type I receptors only, and incorporated an inhibitory protein, Smad7, to implement a simplistic feedback loop. A more recent contribution from Zi and Klipp (13) offered more detailed receptor trafficking than the Vilar model, and incorporated a simplified Smad-pathway and ligand-induced receptor inhibition. The latest model by Schmierer *et al.* (14) focused on Smad nucleocytoplasmic dynamics, providing a better description of the Smad pathway than the Clarke model; but the model still lacks a detailed description of the dynamic process of receptor trafficking and TGF-β-induced receptor activation.

Thus, while these previous modeling efforts have provided adequate descriptions of various aspects of the TGF-β signaling pathway, none provides a sufficiently comprehensive and/or realistic description of the entire system, limiting their ability to facilitate understanding and analysis of the complex TGF-β system and to predict system behavior under aberrant conditions accurately. In particular, the oversimplification or omission of some important steps in the pathway employed in these models limits their suitability for use in attempting to unravel the mystery of the seemingly contradictory roles of TGF-β in cancer progression. Such applications require a more comprehensive and more realistic description of the signaling pathway.

We present in this study, an integrated TGF-β pathway model in epithelial cells, by incorporating transduction of an extracellular signal (i.e. the ligand-binding and the receptor activation and trafficking), transmission of the signal (i.e. the canonical downstream Smad pathway), and by modifying and adding some important mechanisms (sequential receptor activation, protein synthesis, constitutive and ligand-induced degradation of signaling components, nuclear dephosphorylation of Smad, nuclear Smad complex formation, etc.), in accordance with the most up-to-date information available about the TGF-β signaling system. The result, as described below, is a system of ODEs from which, given as input the concentration of the extracellular TGF-β ligand, one obtains as the primary output of interest, the dynamic behavior of the activated Smad2-Smad4 complex in the nucleus, (which ultimately determines target gene expression and cellular responses) along with the dynamics of other intermediate signaling component proteins. Through simulation and model analysis, our integrated model provides insight into the signal-response relationship between the binding of TGF-β to its receptor at the cell surface and the activation of downstream effectors in the signaling cascade. In particular, we use the model to carry out "*in-silico* mutations" from which we generate several hypotheses regarding potential mechanisms for how TGF-β's tumor-suppressive roles may appear to morph into tumor-promoting roles.

MATERIALS AND METHODS

Model Development

The following is a description of the essential molecular processes on which the model is based.

The binding of ligand to signaling receptors

The active form of dimeric TGF-β (assumed to be a single unit) binds to the ectodomain of dimeric Type II receptor (TβRII, designated as RII in the kinetic scheme) and forms a catalytically active TGF-β-RII complex (designated as TGFβ-RII). The activated TGFβ-RII complex subsequently interacts with Type I receptor (TβRI or ALK5, designated as RI), and activates it, forming a TGFβ-RII-RI complex (designated as R^C) at the cell surface (1), which is ready for downstream signaling.

Receptor internalization and recycling

It has been reported that TGF-β receptors are continuously internalized via clathrin-coated pits into early endosomes and are recycled to the plasma membrane for signaling, even in the absence of ligand (15, 16). Vilar *et al*. (10) have modeled the dynamic behavior of TGF-β receptors, considering receptor internalization and recycling. We adopt the approach of Vilar and coworkers, using first-order kinetics to describe receptor trafficking.

Smad phosphorylation

Although the receptors for TGF-β signal through both Smad2 and Smad3 proteins in epithelial cells, we select Smad2 to represent the R-Smads, because the two are virtually identical kinetically; furthermore, Smad2 is ~12-fold more abundant than Smad3 (11, 17). Based on previous studies showing that Smad activation for signaling requires internalization of the TGF-β receptor (15, 18, 19), we assume that Smad2 in the cytoplasm interacts first with the activated ligand-receptor complexes internalized into early endosomes, and then is phosphorylated.

Smad heteromerization

The stoichiometry of active R-Smad/Smad4 heteromeric complexes is still a controversial topic; the R-Smad/Smad4 complexes have been suggested to function as either dimers or trimers (20-25). For simplicity, we assume that phosphorylated Smad2 and Smad4 form a heterodimeric complex. In principle, receptor-activated R-Smads could associate with Smad4 in the cytoplasm first, followed by their entry into the nucleus as RSmad-Smad4 complexes; alternatively, these complexes could form *after* R-Smads translocate into the nucleus (26, 27). The latter implies nuclear import of monomeric phosphorylated R-Smads, which is discussed next.

Nucleocytoplasmic shuttling

In the basal state, both R-Smads and Smad4 are predominantly localized in the cytoplasm. However, upon ligand stimulation, both species rapidly accumulate in the nucleus (27, 28). It is becoming clear that these distributions are not static; rather both R-Smads and Smad4 shuttle continuously between the cytoplasm and nucleus regardless of TGF-β stimulation, ultimately reaching a dynamic equilibrium (17, 29-31). We therefore consider both import and export steps for monomeric R-Smad and Smad4 in our model. Although it is widely believed that activated R-Smads translocate into the nucleus in the heteromeric complex form with Smad4, it has been observed that complex formation of TGF-β-induced R-Smads with Smad4 is not always necessary for their accumulation in the nucleus (27, 32, 33). We therefore include nuclear import of receptor-phosphorylated R-Smad monomers in the cytoplasm in the model.

It has been suggested that the nuclear export signal (NES) of Smad4 may be masked through complex formation with activated R-Smads (2, 17, 27), resulting in nuclear accumulation of Smad4 after TGF-β stimulation. Also, a recent study proposed that only monomeric unphosphorylated Smad2 is capable of export so that the phosphorylated complex form of Smad2 is trapped in the nucleus (29). These observations provide the basis for our assumption that translocation of activated monomeric R-Smads and heteromeric RSmad-Smad4 complex is unidirectional.

Developing realistic mathematical descriptions of nucleocytoplasmic shuttling of Smads has been complicated by the complexity of, and uncertainty associated with, the import and export mechanisms that depend on the type of R-Smads. For example, regarding nuclear import, it has been proposed that Smad2, Smad3, and Smad4 enter the nucleus by direct interactions with the nuclear pore complex (34, 35). However, it also has been suggested that the nuclear import of Smad3 and Smad4 depends on the nuclear import factor, importin-β (36, 37). On the other hand, Smad4 export from the nucleus is mediated by CRM-1 (chromosomal region maintenance-1) nuclear export factor, whereas R-Smad export is independent of CRM-1 and simply may be mediated by direct interactions with nucleoporins (34, 35). In the absence of a consensus, we opt for a simple mechanism of nucleocytoplasmic shuttling, assuming first-order kinetics for both import and export steps.

Dissociation and Dephosphorylation

Suspecting the existence of unidentified R-Smad phosphatases, it has been proposed that R-Smads should undergo cycles of phosphorylation and dephosphorylation to shuttle between the cytoplasm and the nucleus in the presence of a TGF-β signal (17, 27, 29, 31). Lin *et al.* (38) recently confirmed this postulate about the existence of the phosphatases by identifying a Smad-specific phosphatase, PPM1A, that directly dephosphorylates Smad2 and Smad3 to limit their activation. Thus, it is believed that dephosphorylation of Smad2 by the phosphatase leads to dissociation of R-Smad-Smad4 complexes to terminate the TGF-β signaling upon receptor deactivation, or to recycle R-Smads in the presence of a prolonged TGF-β signal, implying that dephosphorylation precedes dissociation. However, because a receptor-phosphorylated R-Smad monomer also may form a complex with Smad4 after R-Smads translocate into the nucleus as well as in the cytoplasm, we cannot rule out the possibility of activated Smad complex dissociating prior to dephosphorylation (39). We therefore include both steps in our model. It has been reported that PPM1A is primarily localized in the nucleus regardless of TGF-β stimulation (38), which supports the previous suggestions that R-Smad dephosphorylation seems to occur in the nucleus (26, 31). This leads us to take only nuclear dephosphorylation into account in our model.

Protein degradation

Each signaling component in the pathway is irreversibly eliminated via different mechanisms. First, degradation of receptors can occur via two different modes: ligand-dependent degradation targeted by Smad7-Smurf2 via the lipid-raft caveolar pathway, and ligand-independent (or constitutive) degradation (10, 16). We assume that ligand-unbound Type I and Type II receptors, and ligand-induced receptor complexes at the surface are terminated in the pathway, as suggested by Vilar *et al.* (10). Secondly, it has been reported that receptor-activated Smad2 undergoes TGF-β-induced, ubiquitin-dependent degradation (40). It also has been suggested that proteasomal degradation of Smad2 is likely to occur in the nucleus, mediated by

the interaction of Smurf2 with phosphorylated Smad2 (41), whereas Smurf2 is known as a cytoplasmic protein (42). Thus, it remains unclear whether Smad2 is targeted to either nuclear or cytoplasmic proteasomes or both. In this study, we assume that monomeric receptor-phosphorylated Smad2 is irreversibly removed by nuclear proteasomes, and un- and/or de-phosphorylated single Smad2 is eliminated in the cytoplasm. Lastly, it has been reported that ubiquitination and proteasomal degradation of Smad4 is mediated by its direct interaction with Jab1, known as a coactivator of c-Jun and subunit of COP9 signalosome (43). We assume that Smad4 is eliminated in the cytoplasm.

Protein synthesis

Describing the production of proteins in a mathematical manner is quite complicated because of the uncertainty and complexity of the nuclear mechanisms for gene expression. Alternatively, many mathematical models of cell signaling which deal with proteins alone assume constant production of the signaling components (10, 12, 44)., Likewise we also assume that the 4 major signaling components (i.e. Type I and Type II receptors, Smad2, and Smad4) are produced under stationary conditions regardless of the presence of ligand.

The components of the overall TGF-β signaling pathway as featured in our model are depicted in Figure 1. The resulting model is a system of 17 non-linear ordinary differential equations (ODEs) with 37 kinetic parameters arising from chemical reactions represented by mass action kinetics. The complete set of model equations, shown in Table 1, is integrated using the ODE15s routine of MATLAB 7.1 (The MathWorks, Inc.).

Our model is based on three well-mixed compartments with the basic cellular characteristics defined for human keratinocyte HaCaT cells as follows: the extracellular (calculated as 1 mL/10^6 cells), the cytoplasmic, and the nuclear compartments. The cell is idealized as a sphere with a diameter of 15 μm, resulting in a cell volume of 1.5×10^{-12} L. Since, according to (29), an average cytoplasmic/nuclear volume ratio for HaCaT cells is approximately 3, we choose the values 1.13×10^{-12} L and 3.75×10^{-13} L, respectively, for the volumes of the cytoplasmic and nuclear compartments.

Initial conditions

We select the value 10,000 for the total number of TGF-β receptor molecules in the basal state. (This number is the median of the values presented in the literature (45)). Assuming that Type I and Type II receptors are evenly distributed, we choose the value 5,000 each for the initial number of Type I and Type II receptor molecules. From recent observations that receptors are continuously internalized and recycled to the surface whether ligand is present or not, we assume that only 10% of total receptors are present in the plasma membrane at any one time and that the remaining 90% of total receptors are sequestered in endosomes (10, 15, 16). We also select a total number of 100,000 each for Smad2 and Smad4 molecules (11). In the basal state, 15% of total Smad2 and 13% of total Smad4 are assumed to reside in the nucleus (29). All other species are set to zero initially.

Model parameter estimation

To carry out simulations with the model requires specific values for the reaction kinetic parameters. Parameter estimation, the procedure for determining from a set of experimental data the values of unknown model parameters, continues to receive attention in systems biology. However, currently there is no consensus as to how to deal with such important related issues as

parameter identifiability, the possibility of multiple local minima, and high computational costs. The approach taken in this present work is summarized as follows:

1. *Initial Rough Estimation*: Several kinetic parameter values were determined through an extensive literature search; some were computed using available *in vitro* experimental data; we also used physical constraints to determine others. For instance, the dissociation constant $K_d=k^{off}/k^{on}$ is available for protein-protein binding reactions, whereas the separate on- and off-rates, k^{on} and k^{off}, are not. Under these conditions, we chose an initial estimate for k^{on} by comparison with similar steps in other kinase pathways and computed the corresponding k^{off} as $k^{off}=K_d \times k^{on}$. The remaining unknown parameters were provided with initial estimates and reasonable upper and lower bounds by comparison with similar circumstances in the literature (e.g. similar steps in previous models or other signaling pathway models) and from known physical limitations (e.g. the diffusion-limited rates, 10^8-10^9 $M^{-1}s^{-1}$ (46)).

2. *Parametric Sensitivity Analysis*: To identify which parameters are the most important and which must therefore be estimated most precisely, using the set of initial estimates determined in Step 1 above, we performed local parameter sensitivity analysis to determine the effect of parametric changes on the set of five system responses of interest for which experimental measurements are available (i.e. total Smad2 in the nucleus and the cytoplasm (27), total phosphorylated Smad2 in the nucleus and the cytoplasm (17, 27), and total Smad4 in the nucleus (27)). The computations are based on the following expression for the normalized sensitivity coefficient (NSC):

$$NSC_{ij}(t) = \frac{p_j}{y_i}\frac{\partial y_i(t,\mathbf{p})}{\partial p_j}\bigg|_{\mathbf{p}}, \qquad i = 1,2,\ldots,5; \qquad j = 1,\ldots,37$$

where y and **p** respectively denote the system response variables and kinetic parameters. A total of 13 parameters were selected to be estimated more precisely because of their high sensitivity coefficients and/or because we had little or no confidence in their initial values.

3. *Least Squares Fitting to Data*: We fit our model predictions simultaneously to corresponding *in vitro* experimental data from the literature, via local minimization of the sum of squared residual errors:

$$\min_i R(\mathbf{p}) = \frac{1}{2}\sum (y_i(t,\mathbf{p}) - y_i^*(t))^2$$

where $y_i(t,\mathbf{p})$ and $y_i(t)$ denote, respectively, model predictions for a given trial of parameter values, **p**, and the corresponding experimental measurements, for each measured variable, *i*. The experimental data used for the curve-fitting are time courses of (i) total Smad2 in the nucleus (27), (ii) total Smad2 in the cytoplasm (27), (ii) total phosphorylated Smad2 in the nucleus (17), (iv) total phosphorylated Smad2 in the cytoplasm (27), and (v) total Smad4 in the nucleus (27). We quantified the immunoblot literature data with the Image Processing Toolbox in MATLAB 7.1, and normalized both the experimental data and the corresponding model estimates to the largest intensity point of each data set. The optimum parameter values (constrained to lie within the specified upper and lower bounds) were determined using the nonlinear least square '*lsqnonlin*' routine of MATLAB 7.1.

4. *Identifiability*: We performed a "practical identifiability" analysis to determine whether the unknown parameters of the postulated model can be uniquely estimated from the available data, following Birtwistle *et al.* (47). Briefly, approximate local confidence intervals for the parameter set are given by,

$$CI_i = t_{\alpha/2}^{N_t - N_p} \sqrt{\frac{S}{N_t - N_p}} \sqrt{(\mathbf{Z}^T \mathbf{Z})_{ii}^{-1}}$$

where N_t and N_p respectively denote the number of experimental data time points and the number of parameters to be estimated; $t_{\alpha/2}^{N_t - N_p}$ is the Student's *t*-distribution statistic evaluated with N_t-N_p degrees of freedom, at confidence level 100(1- α)%, (with α as the "tail area probability" typically set at 0.05 to yield a 95% confidence level); *S* is the sum of squared errors, and $\boldsymbol{Z}$ is the model sensitivity matrix evaluated at the current parameter values. The i^{th} parameter is said to be *practically locally identifiable* only if the magnitude of its approximate confidence interval is less than a specified tolerance i.e. $|CI_i| < \varepsilon_i$. We chose tolerances such that the approximate confidence intervals on identifiable parameters were generously set at ± ~40%.

5. *Identifiable Parameter Estimate Refinement*: Estimated values for identifiable parameters were further refined by repeating Step 4 (local identifiability test) followed by Step 3 (local least squares estimation). After obtaining the "best" estimates of this subset of parameters, we carried out a final least squares estimation of the entire parameter set.

The results of this procedure (final estimates as well as the identifiability status of each parameter) are listed in Table 2.

RESULTS AND DISCUSSION

Model Development and Validation

Model fit to literature data

A comparison of the model fit to the five sets of *in vitro* experimental data used for parameter estimation is shown in Figures 2A-E. First, Fig 2A shows the model fit to data on total nuclear pSmad2 reported by Inman *et al.* (17) in response to a step input of 2ng/ml of TGF-β. Note the good agreement between the model prediction and the data. Furthermore, this dynamic profile also agrees well with other reported experimental results that show the level of nuclear pSmad2 peaking approximately 45-60 min after TGF-β treatment and declining thereafter, but not to zero, even after 6-8 hours (27, 48). The model fit to total cytoplasmic pSmad2 data under conditions where protein synthesis is strongly inhibited in the cells, as reported in Pierreux *et al.* (27), is shown in Fig. 2B. The model shows that the level of cytoplasmic pSmad2 drops sharply after peaking rapidly, and remains very low thereafter. Considering that receptor-activated Smad2 resides either in the cytoplasmic or in the nuclear compartment, it appears as if more of pSmad2 accumulates in the nucleus during active signaling of TGF-β (17, 29-31) than elsewhere.

Next, Figs 2C and 2D show the model fit to experimental profiles of total Smad2 in the nucleus and the cytoplasm, respectively, under the conditions where cells were treated continuously with 2ng/mL of TGF-β and 20 μg of protein synthesis inhibitor, cycloheximide

(27). Note how the dynamic pattern of the nuclear Smad2 response appears to be the opposite of the cytoplasmic response. In other words, while the level of nuclear Smad2 reaches a peak and decreases thereafter, the amount of cytoplasmic Smad2 drops correspondingly and then increases. These opposite dynamics may be caused by the shuttling of Smad2 between the cytoplasm and the nucleus via a mechanism that involves the steps of nuclear import and export of Smads; association between nuclear pSmad2 and Smad4; dissociation of the complex; and dephosphorylation of the activated Smad2, and (re)phosphorylation of Smad2 by active receptors.

Finally, Figure 2E shows the model fit to experimental data from Pierreux *et al.* (27) for total nuclear Smad4 in response to a step of 2ng/mL of TGF-β. Although Smad4 shuttles continuously between the cytoplasm and the nucleus in the absence of ligand, TGF-β stimulation allows Smad4 to reside more in the nucleus than in the cytoplasm through complex formation with pSmad2. However, nuclear events such as dephosphorylation of pSmad and dissociation of Smad complex allow nuclear Smad4 to return to the cytoplasm. Thus, nuclear Smad4 reaches peak activity at approximately 0.5-2 hr after ligand addition and declines thereafter (27).

Keeping in mind that the model was fit to these five data sets *simultaneously*, the resulting agreement between model prediction and data is quite good overall. The inevitable discrepancies between model prediction and experimental data are attributable to the following factors. First, the data sets are from different laboratories and were therefore acquired under non-identical conditions (e.g. cell culture conditions, cell population, etc). Thus, model parameters that may be appropriate for one set of experimental data may not be entirely appropriate for another. The optimum model parameters will therefore result from compromises whereby an otherwise "better" fit to a single data set is traded off for a reasonable fit to the complete collection. Next, values for kinetic parameters (e.g. dissociation constants, Michaelis constants, etc) determined from *in vitro* measurements reported in the literature and used in the model may not exactly correspond to values that obtain under *in vivo* experimental conditions. Finally, to a lesser extent, the model non-linearity and constraints raise the distinct possibility that the resulting optimum parameter set may have been found in a local minimum. While it is possible to address this problem by using such global optimization methods as Genetic Algorithm and Simulated Annealing, it is not clear that the additional and quite significant computational cost is justifiable in this case. Taking all of these considerations into account, the model does a reasonable job of capturing the dynamic behavior of TGF-β signaling as reported in the experimental literature.

Model Validation

Because the data sets shown in Figs 2A-E were used to determine unknown model parameters by minimizing the sum of squared differences between model prediction and data, it is important, before proceeding to use the model, to validate its prediction against a different set of independent experimental data, without adjusting any model parameters. To validate our model in this manner, we compared its predictions to four independent experimental data sets obtained from the literature: (i) total phosphorylated Smad2 in the cell (40), (ii) ratio of cellular pSmad2 to total Smad2 in response a step input in the ligand concentration, (iii) same as in (ii) except in response to a rectangular pulse input (38), and (iv) total Smad4 in the cytoplasm (27).

Figure 3A shows the predicted dynamics of total cellular (cytoplasmic + nuclear) Smad2 phosphorylation in response to a step input of 200 pM of TGF-β, compared to the corresponding experimental observations reported in Lo and Massague (40). The model prediction, especially

the early response, shows remarkably good agreement with the data, even though its deviation from data becomes somewhat more pronounced with time after the peak.

A model prediction of the ratio of pSmad level to total Smad in response to a step input of 2ng/ml of TGF-β is shown in Figure 3B compared to the experimental data of Lin *et al.* (38). Again, the agreement between model prediction and data is very good, with the prediction falling within the experimental error bars. How the ratio of pSmad2 level to total Smad2 responds to a short rectangular pulse of 2 ng/ml of TGF-β followed by TβRI kinase inhibitor SB431542 to block further phosphorylation (38) is shown in Figure 3C, where the model prediction is seen to match the data almost perfectly.

Finally, for cells induced by a step input of 2ng/ml of TGF-β and treated by 20 μg of protein synthesis inhibitor, cycloheximide (27), Figure 3D shows the agreement between the model prediction of cytoplasmic Smad4 response and the experimental data.

Overall, given that these are results of *direct* model predictions of four separate and independent experimental data sets, with no model parameter adjustments, we conclude that the model represents the dynamic behavior of the TGF-β signaling pathway quite well.

Model Analysis and Simulation

In this section, we present results of computational "experiments" used to explore the dynamic behavior of the now-validated TGF-β signaling model. From among several signaling components in the pathway, we select phosphorylated Smad complex in the nucleus and to represent the signaling activity of the TGF-β pathway, since the expression of TGF-β-inducible genes is regulated by nuclear activated Smads. The premise is that such computational investigations into the dynamics of the TGF-β-induced Smad complex in the nucleus, under various conditions, will facilitate understanding and characterization of the TGF-β/Smad pathway; it also will provide clues regarding the role(s) of this pathway in tumor progression and metastasis. All simulations were performed with the parameter values in Table 2, and step inputs of 80 pM of TGF-β, unless otherwise specified.

Model parameter sensitivity analysis

While parameter sensitivity analysis has been shown to play an important role in parameter estimation, it also can be employed to obtain insight into the model behavior itself. Specifically, sensitivity analysis carried out for the primary output of interest, nuclear pSmad2-Smad4 complex, will help us understand quantitatively which aspects of the pathway most affect the system behavior.

Figure 4 shows normalized sensitivity coefficients as a function of time for the 10 most important parameters (parameters for which the maximum normalized sensitivity coefficient exceeds 0.5 in absolute value at any point in time). The most important features of this plot are summarized as follows: (1) Immediately after ligand stimulation, the output variable is strongly affected by four of this set of most sensitive parameters: in order of importance, these are k_{4a} (binding of Smad2 to active receptors), k_{3int} (internalization of receptor complexes), k_{7imp} (nuclear import of pSmad2-Smad4), and k_{2a} (complex formation of activated TβRII and TβRI). (2) On the other hand, in the mid- to longer time interval following ligand stimulation, the following parameters become more important: in order of importance, these are k_{18a} (association of nuclear pSmad2 and Smad4), and k_{18d} (dissociation of nuclear pSmad2-Smad4), k_{11exp} (nuclear export of Smad4), k_{20lid} (ligand-induced degradation of pSmad2), k_{11imp} (nuclear import

of Smad4), k_{23rec} (recycling of internalized receptor complexes), k_{3int} (internalization of receptor complexes), and k_{4a} (binding of Smad2 to active receptors).

These results have biologically important consequences. First, the high sensitivity coefficients of the receptor-related parameters (i.e. k_{2a}, k_{3int}, k_{4a}, and k_{23rec}) reveal that the system responses to TGF-β are highly dependent on the active state of the receptors. In particular, Figure 4 shows that 45-60 min after TGF-β treatment, by which time nuclear pSmad2-Smad4 would have reached its peak activity (Figure 2A), the importance of the state of ligand-activated receptors on the species again increases. Considering that nuclear pSmad2-Smad4 complex loses its activity by dephosphorylation and is destroyed by proteasomal degradation, this result implies that to maintain accumulation of activated Smad complex in the nucleus, R-Smad must be continuously phosphorylated by active receptors. Taking into account that after ligand stimulation, free Smads in the cytoplasm are either still unphosphorylated or have been exported from the nucleus after undergoing dephosphorylation, this result reveals that the mechanism involving rephosphorylation of Smad plays a vital role in the nuclear accumulation of pSmad2-Smad4, especially at post-peak times. To recycle Smad2 for rephosphorylation during active signaling, nuclear pSmad2 (either monomeric or heteromeric) must undergo dephosphorylation by phosphatases because only monomeric unphosphorylated Smad2 is capable of export from the nucleus to the cytoplasm so that the phosphorylated complexed form of Smad2 is trapped in the nucleus (29). Although the sensitivity analysis shows that nuclear pSmad2 complex is less sensitive to changes in the dephosphorylation step, this step is indispensable to the recycling of Smad2. To conclude, the parametric sensitivity analysis shows that the mechanisms for Smad2 recycling (i.e. phosphorylation-dephosphorylation-rephosphorylation) have a critical effect on the transcriptional activity of the signaling pathway.

The increasing nature of the sensitivity coefficients of k_{18a} and k_{18d} over time shows that *both* the formation of pSmad2-Smad4 complex in the nucleus and its dissolution are crucial for nuclear retention of these complexes. Our model has two sources of monomeric pSmad2 in the nucleus. One source is the dissociation of pSmad2-Smad4 complexes that are formed in the cytoplasm and then translocated to the nucleus; the other is nuclear entry of monomeric Smad2 that was phosphorylated in the cytoplasm. The former requires effective nuclear translocation of pSmad2-Smad4 complexes, as confirmed by the high sensitivity coefficient of the parameter k_{7imp}. Unlike other parameters, however, the effect of the nuclear import of activated Smad complexes is not significant over longer periods. On the other hand, considering that the importance of k_{18a} and k_{18d} increases over time (see Figure 4), it is likely that the latter source, the nuclear import of cytoplasmic monomeric pSmad2, also plays a vital role in the nuclear retention of pSmad2-Smad4 complexes. To confirm this, we computationally "blocked" the nuclear import of pSmad2-Smad4 complexes while allowing import of pSmad2 monomer, and then prevented nuclear import of pSmad2 monomer while allowing import of the complexed pSmad in order to study the effects of these "blockades" on the nuclear accumulation of active Smad complexes. Figure 5 shows that the effect of blocking the nuclear import of cytoplasmic pSmad2-Smad4 complexes (i.e. the effect of nuclear complex formation between pSmad2 and Smad4) on nuclear retention of active Smad complexes is not trivial compared to the effect of preventing the nuclear entry of monomeric pSmad2. Taking the importance of Smad4 for nuclear complex formation into account, it is not surprising that the significance of nucleocytoplasmic shuttling of Smad4 (k_{11imp} and k_{11exp}) increases at longer times. Many biological "models" of the pathway mechanisms have neglected the nuclear entry of monomeric pSmads and the nuclear

complex formation between Smad2 and Smad4, but this result argues strongly for their incorporation.

The effect of Smad phosphorylation

As seen in previous sections, the nuclear accumulation of Smad2-Smad4 complexes is significantly affected by the dynamics of activated receptor complexes. To examine how variations in the active state of receptors influence the nuclear retention of pSmad2 complexes, we varied the rate of the binding between ligand-activated receptor complexes and Smad2 in the cytoplasm (k_{4a}) 10-fold, because the dynamics of the activated receptor complexes are ultimately reflected in the phosphorylation of Smad2 for downstream signaling. Because it has been reported that Smad7, one of the inhibitory Smads, can bind to activated receptors in competition with R-Smads (26, 49, 50), this simulation may also provide insight into the inhibitory effect of Smad7 on TGF-β signaling. Figure 6A shows that when complex formation between ligand-activated receptors and Smad2 occurs more rapidly, more pSmad2 complexes are accumulated in the nucleus for a longer period, and the time to achieve peak accumulation of nuclear pSmad2 is shortened somewhat. Conversely, the slower binding of Smad2 to the receptors induces lower and slower accumulation of pSmad2 in the nucleus. These results suggest that regulation of the active state of the ligand-activated receptors and their complex formation with R-Smads may significantly affect the system responses to TGF-β through the nuclear retention of pSmad2 complexes in terms of the intensity and the duration of transcriptional activity.

The effect of nuclear Smad complex formation

We also investigated how Smad complex formation in the nucleus affects nuclear accumulation of activated Smad complexes, by varying the rate of association between nuclear pSmad2 and Smad4 (k_{18a}) 10-fold (Figure 6B). The results show that while rapid formation of the complex between nuclear pSmad2 and Smad4 induces prolonged and enhanced nuclear accumulation of pSmad2-Smad4 complex, slow binding of pSmad2 and Smad4 leads to shortened and attenuated retention of pSmad2 complex in the nucleus. Thus, these results imply that the nuclear complex formation step plays an important role in regulating the intensity and duration of TGF-β-targeted transcriptional activities through pSmad2 complexes. More importantly, the results imply that pSmad2 complex-mediated response to TGF-β stimulation may be significantly attenuated by competitive inhibition or by interference from other nuclear molecules that also have high affinity for either pSmad2 or Smad4. This inhibitory action ultimately gives rise to a significant reduction in the rate of association between these proteins. This conclusion is supported by a recent finding that a ubiquitous nuclear protein, transcriptional intermediary factor 1γ (TIF1γ), selectively binds receptor-phosphorylated Smad2/3 in competition with Smad4 (51, 52). There is also the possibility that other molecules not yet identified may bind to either pSmad2 or Smad4 with high affinity; these putative molecules then would hamper complex formation between pSmad2 and Smad4. Taken together, these results reveal that the step of complex formation between pSmad2 and Smad4 is closely associated with modulation of TGF-β-induced signal patterns.

The effect of signal turn-off

Inactivation of ligand-activated R-Smads is crucial for controlling the extent of TGF-β effects. In our model, irreversible inactivation and termination of the pSmad2-mediated signals can be achieved in one of two ways: (i) via ligand-induced ubiquitination and subsequent

degradation by proteasomes, or (ii) via dephosphorylation by inorganic phosphatases. We examined the effect of ligand-induced degradation of nuclear pSmad2 on the nuclear retention of pSmad2 complexes by changing the rate constant (k_{20lid}) 10-fold. Figure 6C shows that slower degradation of pSmad2 results in higher and more sustained activity of nuclear pSmad2 complexes. On the other hand, when the rate of degradation is increased, the activity of pSmad2 complexes in the nucleus decreases more rapidly immediately after attaining its peak value, dropping almost to zero in the long term, hence resulting in transient dynamics. Taken together with the previous sensitivity analysis results, these simulations reveal that ligand-induced multi-ubiquitination via Smurf2 protein and subsequent degradation of activated Smad2 by proteasomes can play a vital role in regulating TGF-β-dependent transcription.

Similar system responses were obtained when the rates of pSmad2 dephosphorylation (k_{8dp} and k_{19dp}) were changed 10-fold (Figure 6D). When pSmad2 dephosphorylation occurred faster, the peak activity of nuclear pSmad2 complexes was noticeably reduced and the activity reached steady state more rapidly. However, the results show that variations in the dephosphorylation rates also changed the intensity of the response, but did not significantly affect the signal duration. This is because dephosphorylation by phosphatases can affect only the activity of nuclear Smads, and not the irreversible termination of the component itself. In other words, even though nuclear pSmads lose their activity by dephosphorylation, they can be rephosphorylated after exiting the nucleus, as long as the receptor activated signaling pathways remain active. These results therefore indicate that ligand-induced ubiquitination and subsequent proteasomal degradation can play an important role in regulating *both* the duration and intensity of Smad-mediated signal responses to TGF-β, whereas dephosphorylation may have a significant effect only on the signal intensity.

The effect of inhibiting nuclear import of active Smads

It has been reported that Smad activity can be regulated by diverse extracellular signal inputs through corresponding kinase pathways (3, 6). One of the interactions between Smad and other pathways is achieved by direct phosphorylation of the linker region connecting the MH1 and MH2 domains of Smad proteins. This region is phosphorylated by endogenous mitogen-activated protein kinase (MAPK), Ca^{2+}-calmodulin-dependent protein kinase II (CamKII), and cyclin-dependent kinases (CDKs). These inputs attenuate the nuclear accumulation and transcriptional activity of Smads, and negatively impact TGF-β signaling function. Although our model is limited in its ability to investigate all possible effects of crosstalk between TGF-β and other signaling pathways, still we are able to examine the effect of such input signals on the nuclear accumulation of Smads by directly varying the rate of nuclear import of TGF-β-activated Smads. Figure 6E shows that a large (10-fold) increase in the rates of nuclear translocation of both monomeric and complexed pSmad2 (k_{7imp} and k_{17imp}) does not have a pronounced effect on the nuclear retention of Smads. A 10-fold decrease in the rates resulted in a reduced response, but its effect is relatively insignificant, compared with the effects of variations in the parameter values of other important steps in the pathway. The immediate implication is that nuclear retention of Smads is relatively insensitive to crosstalk between Smad and other kinase pathways through phosphorylation of the Smad linker and consecutive inhibition of their entry to the nucleus.

TGF-β-dose-dependent responses

We examined the effect of various TGF-β concentrations on the dynamics of the signaling system. Step inputs of four different concentrations of TGF-β (0.02, 0.2, 2, and 20 pM) were used to investigate the dose effects. All other conditions, including the initial conditions and kinetic parameters, remained the same. Figure 7A shows that as the TGF-β concentration increases, the activity of receptor complexes also increases and the peak activity time increases somewhat. Increases in TGF-β concentration also enhanced activity of receptor-activated Smad complexes and induced faster kinetics for active Smad complexes by allowing Smads to reach peak activity somewhat more rapidly (Figure 7B). For instance, while 0.02 pM of TGF-β induced maximum activity of Smads in 93 min, 20 pM of TGF-β resulted in peak activity of Smad in 54 min. Considering that activated Smad complexes in the nucleus regulate expression of TGF-β-target genes, these results reveal that an increase in the concentration of TGF-β may accelerate and enhance Smad-mediated cellular responses.

It is important to note that as the TGF-β concentration increases, the observed differences in the signaling activity diminish. For example, the response to a 2 pM stimulus is not significantly different from that for a 20 pM stimulus. This observation is true for both receptors and Smads. These results reveal that there is a saturation concentration of TGF-β above which Smad-mediated signaling responses within a cell no longer change. In other words, no matter how many bioactive TGF-β molecules are available in the extracellular space, each cell has a receptor-limited capacity to respond to them and consequently induce the corresponding signal responses.

In-silico mutations

How can cancer cells become resistant to the tumor-suppressor effects of TGF-β, but, at the same time, remain responsive to the tumor-promoter effects? We believe that differences between normal and cancerous signaling responses could offer some clues.

It is known that some signaling effectors of the TGF-β pathway are abnormally altered in many human tumors (53). Specifically, aberrant alterations such as mutations, deletions, and downregulation of Type I and/or Type II receptors are most frequently observed in a variety of human cancers including prostate, breast, ovarian, bladder, gastric, and pancreatic cancer. We have therefore investigated the effect on the TGF-β signaling system of some of these common abnormal alterations in receptors, using a 10-fold reduction in the initial levels and production rate of both Type I and Type II to represent cancerous conditions.

First, Figures 7C and 7D show the TGF-β dose-dependent responses for cancerous cells, corresponding to what was shown earlier in Figs 7A and 7B for normal cells. While a comparison of Figs 7A and 7C reveals only slight differences in the relative activity of receptor complexes for normal and cancerous cells, the situation is different with the nuclear Smad-mediated activity. A careful comparison of Figs 7B and 7D indicates that the amount of TGF-β needed to produce saturated Smad-mediated response in cancer cells is far higher than that in healthy cells. Specifically, the response in Figure 7B for normal cells is essentially saturated with 0.2 pM of TGF-β (with higher doses producing essentially the same response); Fig 7D on the other hand shows that at least 2 pM of TGF-β is required before the Smad-mediated response begins to approach saturation. This is, of course, a direct effect of the reduction in the number of functional receptors in cancer cells (53) which renders the them less responsive to TGF-β stimulation. But this finding also indicates an important characteristic of cancerous cells: to elicit nuclear Smad-mediated activity generally requires *more* TGF-β than normal.

Next, a head-to-head comparison of normal versus cancerous cell responses reveals some very interesting features. Figure 8A shows that when the level of functional receptors is very low, the activity of ligand-activated receptor complexes (in response to a step of 2 ng/mL, or 80 pM TGF-β) is significantly attenuated compared to that in the normal system. Specifically, the peak level of active receptors in the cancerous system plunges by an astounding 92%. Thus, even though the dose-response characteristics of active receptors are essentially similar for both classes of cells, the actual peak level attained is significantly lower for cancer cells. Once again, this is consistent with what one would expect from cells having fewer functional receptors (53).

Not surprisingly, due to the correlation between active receptors and nuclear pSmads, Figure 8B shows that the sharp drop in the level of functional receptors in cancer cells leads to a marked decrease in the activity of nuclear pSmad complexes. Compared to the normal cell response, the peak activity of nuclear pSmad complexes in cancer cells was reduced by 65%, with the steady-state activity also remaining comparatively low.

Interestingly, a reduction in the level of receptors also slowed nuclear pSmad responses. While nuclear pSmads in the normal system reached maximum activity in 55 min, their activity under a cancerous condition peaked at 86 min.

These results are consistent with our own experimental observations of Smad2 phosphorylation in some prostate cancer cell lines (i.e. LNCaP and C4-2) as shown in Fig 8C. (A separate assay, not shown, confirmed that both LNCaP and C4-2 cells have low levels of TGF-β Type I and Type II receptor proteins.) While peak activity of phosphorylated R-Smads is attained approximately 1 hr after ligand addition in cells with intact TGF-β signaling machinery (40), the metastatic prostate cancer cells with reduced functional receptors showed peak activity much later, as a result of the slower dynamics of activated Smad2 (Figure 8C). Although the kinetics of pSmad2 in the cancer cells could potentially be affected by many factors (e.g. cancer types, cell lines, cell contexts, etc.), our simulation and experimental results reveal that reduction in the receptor levels, a notable phenotypic difference between normal and cancer cells, is closely associated with differences in the dynamic behavior of the pathway.

Taken together, these results indicate generally that a reduction in the level of functional TGF-β receptors in cancer cells may lead to attenuated and slower TGF-β-stimulated signaling responses via Smad2. The specific implications of the model predictions in Figures 7 and 8 reveal some potentially important findings about TGF-β and cancer cells: (i) cancer cells require *higher* than normal levels of TGF-β in order to elicit significantly attenuated (and much slower) nuclear Smad-mediated activity; (ii) but even the increased levels of TGF-β will never be able to produce Smad-mediated responses that will be anywhere close to normal because of the saturation effect shown in Fig 7D. These characteristics may have significant implications for cancer therapies that are based on targeting TGF-β.

Hypotheses on the dual role of TGF-β

As seen above, the dynamic patterns of major signaling components in cancer cells in response to TGF-β may be quite different from those in normal cells. Such differences may provide clues regarding the role of TGF-β — tumor suppressor or tumor enhancer — during cancer progression. Here, we postulate three testable non-mutually exclusive hypotheses arising from our foregoing analysis of the system dynamics.

Hypothesis (1): Different thresholds for gene expression

As shown above via simulation, cancer cells have attenuated TGF-β-stimulated Smad pathway responses. Such cells have been confirmed experimentally to be resistant to the antiproliferative effect of TGF-β, while showing typical pro-oncogenic responses. Such behavior may be explained in part by the following "threshold hypothesis": in response to TGF-β, growth-inhibitory genes require higher threshold levels of nuclear Smad activity for their expression than genes associated with pro-oncogenic and pro-metastatic effects. In other words, under normal conditions, or in the early stage of cancer progression, the antiproliferative responses to TGF-β are predominant over pro-oncogenic responses. This is because the transcriptional activity of nuclear pSmad is high enough to induce anti-growth gene expression. However, as cancer progresses, this transcriptional activity may decline significantly and thereby hardly exceed the threshold necessary for the expression of growth-inhibition genes. Meanwhile, genes related to tumor-promoting effects may be relatively insensitive to the attenuation of the transcriptional activity by Smads, so that the expression of such genes remains approximately unchanged even under cancerous conditions. As a consequence, the dominance of tumor suppressor genes over the tumor-promoter genes may be blunted in cancer cells. This hypothesis is supported in part by previous experimental observations that cells with reduced TGF-β receptor function showed resistance to the antiproliferative effect of TGF-β, whereas other TGF-β responses were not significantly affected (48, 56-58). We believe that further investigation into differences in the temporal profiles of gene expression and thresholds of anti-growth and pro-oncogenic genes induced by TGF-β will provide some clues regarding the putative dual effects of TGF-β.

Hypothesis (2): Fast degradation of signaling components

It has been suggested that the duration of TGF-β/Smad signaling is a critical determinant for regulating specificity of cellular responses (59). For example, Nicolas and Hill (48) reported that normal epithelial cells (HaCaT and Colo-357) with sustained retention of active Smad in the nucleus (more than 6 hr after TGF-β addition) are sensitive to growth inhibition by TGF-β. In contrast, pancreatic cancer cells (PT45 and Panc-1) showing transient nuclear retention of active Smads (1-2 hr after TGF-β treatment) preferentially evade the growth-inhibitory effects of TGF-β, with no changes to other responses. Thus, it seems likely that the expression profile of TGF-β-inducible genes required for cell cycle arrest may differ depending on the dynamic patterns of nuclear pSmads. Taking into account that such pancreatic cancer cell lines contain low levels of TGF-β Type I receptor protein (48), one may be tempted to conclude that the reduction in receptor levels is responsible for driving the transient accumulation of pSmads in the nucleus to induce alteration in the expression profiles of the anti-growth genes. However, reduced levels of receptors may not be the only factor leading to the experimentally observed short-term signal response to TGF-β. We hypothesize that such transient dynamic behavior of nuclear pSmads results from not only a reduction in receptor levels but also from other mechanisms, especially mechanisms associated with rapid degradation of major signaling components in the pathway. We have already seen responses become transient when the rate of pSmad2 degradation increased (Figure 6C). Alterations in the mechanism(s) involved in degradation of pSmad2 during cancer progression may therefore account for producing transient signal responses to TGF- β.

It also is possible that Smad4 may be a major target for rapid degradation. Western blot analysis (48) showed that whereas the activity of Smad4 is sustained in normal cells during active signaling, Smad4 from nuclear extracts of pancreatic cancer cells shows fairly transient dynamics. We suspect that the transient dynamics of Smad4 in cancer cells result from an

expedited degradation process for Smad4 (Figure 9A). To confirm that such a rapid degradation of these two major signaling components, pSmad2 and Smad4, contributes to the transient dynamics of nuclear pSmad2 under cancerous conditions, we carried out simulations with 10-fold increases in the rate constants for either pSmad2 or Smad4 or both under cancerous conditions where the level of receptors is reduced 10-fold. Figure 9B shows that the increased degradation rate of pSmad2 and/or of Smad4, along with decreased expression of receptors, leads to more attenuated and transient dynamics of activated Smads, compared to the response to a decrease in the level of the receptors alone. This hypothesis is corroborated by previous findings that in response to TGF-β, tumor cells show increased production of proteases and downregulation of the protease inhibitors, leading to rapid degradation of signaling components; these features are not observed in normal cells (60). Further investigations into changes in the degradation mechanisms of the signaling components in the pathway during cancer progression may therefore be important in understanding the apparently contradictory roles of TGF-β.

Hypothesis (3): Competitive inhibition by nuclear binding partner of pSmad

The last hypothesis is related to mechanisms that influence the rate of pSmad2-Smad4 complex formation and/or dissociation, which also affect the duration of TGF-β/Smad signaling. Our sensitivity analysis has shown that association and dissociation between pSmad2 and Smad4 in the nucleus critically affect nuclear accumulation of pSmad2-Smad4 complexes in terms of signal intensity and duration. In particular, Figure 6B shows that retardation of nuclear complex formation of pSmad2 with Smad4 leads to attenuated and transient signal responses. We hypothesize that one possible factor in the sluggishness of pSmad2-Smad4 complex formation is competitive inhibition by other binding partners of ligand-activated Smad in the nucleus, apart from Smad4. This is supported by a recent finding that a ubiquitous nuclear protein, TIF1γ, can selectively bind to ligand-activated Smad2/3, competing with Smad4 (51), a schematic diagram of which is shown in Figure 10. This study suggests the possible existence of hitherto unidentified binding partners that show high affinity for receptor-phosphorylated Smad2.

Such binding partners may not only inhibit complex formation between pSmad2 and Smad4, but may also mediate cellular responses different from those mediated by Smad4. The same study (51) showed that in human hematopoietic progenitor cells, the binding of receptor-phosphorylated Smad2/3 to Smad4 mediates inhibition of proliferation, whereas complex formation of pSmad2/3 with TIF1γ mediates differentiation in response to TGF-β. This result strongly suggests the possibility that the Smad pathway can mediate a variety of cellular responses through its branch pathways, depending on nuclear binding partners of TGF-β-induced R-Smads. In particular, if such putative binding partners can mediate cellular responses contradictory to those mediated by Smad4, this may explain the dual role of TGF-β during cancer progression. Suppose that during cancer progression the rate of complex formation between R-Smads and Smad4 slows because of either lower affinity between those molecules or because of higher affinity between R-Smads and other binding proteins, due to conformational changes by mutations or for other reasons. Suppose as well that such binding proteins strongly mediate tumor-promoting responses such as EMT, invasion, and survival. A decreased rate of complex formation between pSmads and Smad4 in the nucleus can lead to an increased number of free nuclear pSmads that can bind to other nuclear partners; this makes for a higher probability of complex formation between pSmads and other partners. Considering that slow association of pSmad2 with Smad4 leads to attenuated and transient responses (primarily tumor-suppressive ones), increased complex formation between pSmad2 and potential binding factors may cause

higher and prolonged tumor-promoting responses. Consequently, in cancers, an imbalance between tumor-suppressing responses by Smad4 and tumor-promoting responses by potential binding factors may explain the paradox of TGF-β.

CONCLUSIONS

In this work we have presented a mathematical description of the TGF-β signaling pathway that is more comprehensive and more realistic than the previous computational models; it integrates extracellular signal transduction and intracellular signal transmission, and includes some reaction mechanisms modified from previous models to be better aligned with current knowledge of the TGF-β pathway. The model, which shows good fit to multiple sources of experimental data, simultaneously, was also validated against several totally different, independent sets of data from different sources, without adjusting any model parameters. Extensive analysis of the model (parametric sensitivity and model predictions under various physiological conditions) has provided insight into basic characteristics of the TGF-β signaling system.

We believe that our model also yields new insights into the relationship between ligand stimulation and corresponding responses via binding of TGF-β to its receptor at the cell surface and the activation of downstream effectors in the signaling cascade; it also yields new insights into molecular TGF-β-induced response characteristics that distinguish between normal and cancer cells. Furthermore, these results provide some clues that may be helpful in unraveling long-standing questions about the seemingly contradictory roles of TGF-β during cancer progression. However, the model is still has some limitations. We plan to expand the current model first to incorporate the effect of crosstalk among other important signaling cascades, and later gene expression mechanisms. Our future plans also include focusing on prostate cancer (PCa), customizing this computation model for the PCa cell lines available in our laboratory, and using the models for a model-guided experimental study of the role of TGF-β during PCa progression.

ACKNOWLEDGEMENTS

This work was supported by Institution of Multiscale Modeling of Biological Interactions (IMMBI) funded by DOE, and DOD grant PC050554.

REFERENCES

1. Massague, J. 1998. TGF-β signal transduction. Annu Rev Biochem 67:753-791.
2. Shi, Y., and J. Massague. 2003. Mechanisms of TGF-β signaling from cell membrane to the nucleus. Cell 113:685-700.
3. Massague, J., and R. R. Gomis. 2006. The logic of TGFβ signaling. FEBS Lett 580:2811-2820.
4. Massague, J. 2000. How cells read TGF-β signals. Nat Rev Mol Cell Biol 1:169-178.
5. Itoh, S., F. Itoh, M. J. Goumans, and P. Ten Dijke. 2000. Signaling of transforming growth factor-β family members through Smad proteins. Eur J Biochem 267:6954-6967.
6. Feng, X. H., and R. Derynck. 2005. Specificity and versatility in TGF-β signaling through Smads. Annu Rev Cell Dev Biol 21:659-693.
7. Elliott, R. L., and G. C. Blobe. 2005. Role of transforming growth factor β in human cancer. J Clin Oncol 23:2078-2093.
8. Wakefield, L. M., and A. B. Roberts. 2002. TGF-β signaling: positive and negative effects on tumorigenesis. Curr Opin Genet Dev 12:22-29.
9. Pardali, K., and A. Moustakas. 2007. Actions of TGF-β as tumor suppressor and pro-metastatic factor in human cancer. Biochim Biophys Acta 1775:21-62.
10. Vilar, J. M., R. Jansen, and C. Sander. 2006. Signal processing in the TGF-β superfamily ligand-receptor network. PLoS Comput Biol 2:e3.
11. Clarke, D. C., M. D. Betterton, and X. Liu. 2006. Systems theory of Smad signalling. Syst Biol (Stevenage) 153:412-424.
12. Melke, P., H. Jonsson, E. Pardali, P. Ten Dijke, and C. Peterson. 2006. A rate equation approach to elucidate the kinetics and robustness of the TGF-β pathway. Biophys J. 91: 4368-4380.
13. Zi, Z., and E. Klipp. 2007. Constraint-based modeling and kinetic analysis of the Smad dependent TGF-β signaling pathway. PLoS ONE 2:e936.
14. Schmierer, B., A. L. Tournier, P. A. Bates, and C. S. Hill. 2008. Mathematical modeling identifies Smad nucleocytoplasmic shuttling as a dynamic signal-interpreting system. Proc Natl Acad Sci U S A 105:6608-6613.
15. Mitchell, H., A. Choudhury, R. E. Pagano, and E. B. Leof. 2004. Ligand-dependent and -independent transforming growth factor-β receptor recycling regulated by clathrin-mediated endocytosis and Rab11. Mol Biol Cell 15:4166-4178.
16. Di Guglielmo, G. M., C. Le Roy, A. F. Goodfellow, and J. L. Wrana. 2003. Distinct endocytic pathways regulate TGF-β receptor signalling and turnover. Nat Cell Biol 5:410-421.
17. Inman, G. J., F. J. Nicolas, and C. S. Hill. 2002. Nucleocytoplasmic shuttling of Smads 2, 3, and 4 permits sensing of TGFβ receptor activity. Mol Cell 10:283-294.
18. Hayes, S., A. Chawla, and S. Corvera. 2002. TGFβ receptor internalization into EEA1-enriched early endosomes: role in signaling to Smad2. J Cell Biol 158:1239-1249.
19. Penheiter, S. G., H. Mitchell, N. Garamszegi, M. Edens, J. J. Dore, Jr., and E. B. Leof. 2002. Internalization-dependent and -independent requirements for transforming growth factor β receptor signaling via the Smad pathway. Mol Cell Biol 22:4750-4759.

20. Funaba, M., and L. S. Mathews. 2000. Identification and characterization of constitutively active Smad2 mutants: evaluation of formation of Smad complex and subcellular distribution. Mol Endocrinol 14:1583-1591.
21. Wu, J. W., R. Fairman, J. Penry, and Y. Shi. 2001. Formation of a stable heterodimer between Smad2 and Smad4. J Biol Chem 276:20688-20694.
22. Wu, J. W., M. Hu, J. Chai, J. Seoane, M. Huse, C. Li, D. J. Rigotti, S. Kyin, T. W. Muir, R. Fairman, J. Massague, and Y. Shi. 2001. Crystal structure of a phosphorylated Smad2. Recognition of phosphoserine by the MH2 domain and insights on Smad function in TGF-β signaling. Mol Cell 8:1277-1289.
23. Chacko, B. M., B. Y. Qin, A. Tiwari, G. Shi, S. Lam, L. J. Hayward, M. De Caestecker, and K. Lin. 2004. Structural basis of heteromeric Smad protein assembly in TGF-β signaling. Mol Cell 15:813-823.
24. Kawabata, M., H. Inoue, A. Hanyu, T. Imamura, and K. Miyazono. 1998. Smad proteins exist as monomers in vivo and undergo homo- and hetero-oligomerization upon activation by serine/threonine kinase receptors. Embo J 17:4056-4065.
25. Jayaraman, L., and J. Massague. 2000. Distinct oligomeric states of SMAD proteins in the transforming growth factor-β pathway. J Biol Chem 275:40710-40717.
26. Massague, J., J. Seoane, and D. Wotton. 2005. Smad transcription factors. Genes & Development 19:2783-2810.
27. Pierreux, C. E., F. J. Nicolas, and C. S. Hill. 2000. Transforming growth factor β-independent shuttling of Smad4 between the cytoplasm and nucleus. Mol Cell Biol 20:9041-9054.
28. Reguly, T., and J. L. Wrana. 2003. In or out? The dynamics of Smad nucleocytoplasmic shuttling. Trends Cell Biol 13:216-220.
29. Schmierer, B., and C. S. Hill. 2005. Kinetic analysis of Smad nucleocytoplasmic shuttling reveals a mechanism for transforming growth factor β-dependent nuclear accumulation of Smads. Mol Cell Biol 25:9845-9858.
30. Nicolas, F. J., K. De Bosscher, B. Schmierer, and C. S. Hill. 2004. Analysis of Smad nucleocytoplasmic shuttling in living cells. J Cell Sci 117:4113-4125.
31. Xu, L., Y. Kang, S. Col, and J. Massague. 2002. Smad2 nucleocytoplasmic shuttling by nucleoporins CAN/Nup214 and Nup153 feeds TGFβ signaling complexes in the cytoplasm and nucleus. Mol Cell 10:271-282.
32. De Bosscher, K., C. S. Hill, and F. J. Nicolas. 2004. Molecular and functional consequences of Smad4 C-terminal missense mutations in colorectal tumour cells. Biochem J 379:209-216.
33. Fink, S. P., D. Mikkola, J. K. Willson, and S. Markowitz. 2003. TGF-β-induced nuclear localization of Smad2 and Smad3 in Smad4 null cancer cell lines. Oncogene 22:1317-1323.
34. Xu, L., C. Alarcon, S. Col, and J. Massague. 2003. Distinct domain utilization by Smad3 and Smad4 for nucleoporin interaction and nuclear import. J Biol Chem 278:42569-42577.
35. Xu, L., and J. Massague. 2004. Nucleocytoplasmic shuttling of signal transducers. Nat Rev Mol Cell Biol 5:209-219.
36. Kurisaki, A., S. Kose, Y. Yoneda, C. H. Heldin, and A. Moustakas. 2001. Transforming growth factor-β induces nuclear import of Smad3 in an importin-beta1 and Ran-dependent manner. Mol Biol Cell 12:1079-1091.

37. Xiao, Z., R. Latek, and H. F. Lodish. 2003. An extended bipartite nuclear localization signal in Smad4 is required for its nuclear import and transcriptional activity. Oncogene 22:1057-1069.
38. Lin, X., X. Duan, Y. Y. Liang, Y. Su, K. H. Wrighton, J. Long, M. Hu, C. M. Davis, J. Wang, F. C. Brunicardi, Y. Shi, Y. G. Chen, A. Meng, and X. H. Feng. 2006. PPM1A functions as a Smad phosphatase to terminate TGFβ signaling. Cell 125:915-928.
39. Schmierer, B., and C. S. Hill. 2007. TGFβ-SMAD signal transduction: molecular specificity and functional flexibility. Nat Rev Mol Cell Biol 8:970-982.
40. Lo, R. S., and J. Massague. 1999. Ubiquitin-dependent degradation of TGF-β-activated Smad2. Nat Cell Biol 1:472-478.
41. Lin, X., M. Liang, and X. H. Feng. 2000. Smurf2 is a ubiquitin E3 ligase mediating proteasome-dependent degradation of Smad2 in transforming growth factor-β signaling. J Biol Chem 275:36818-36822.
42. Zhang, Y., C. Chang, D. J. Gehling, A. Hemmati-Brivanlou, and R. Derynck. 2001. Regulation of Smad degradation and activity by Smurf2, an E3 ubiquitin ligase. Proc Natl Acad Sci U S A 98:974-979.
43. Wan, M., X. Cao, Y. Wu, S. Bai, L. Wu, X. Shi, N. Wang, and X. Cao. 2002. Jab1 antagonizes TGF-β signaling by inducing Smad4 degradation. EMBO Rep 3:171-176.
44. Schoeberl, B., C. Eichler-Jonsson, E. D. Gilles, and G. Muller. 2002. Computational modeling of the dynamics of the MAP kinase cascade activated by surface and internalized EGF receptors. Nat Biotechnol 20:370-375.
45. Wakefield, L. M., D. M. Smith, T. Masui, C. C. Harris, and M. B. Sporn. 1987. Distribution and modulation of the cellular receptor for transforming growth factor-β. J Cell Biol 105:965-975.
46. Wilkinson, K. D. 2004. Quantitative analysis of protein-protein interactions. Humana Press, Totowa, N.J.
47. Birtwistle, M. R., M. Hatakeyama, N. Yumoto, B. A. Ogunnaike, J. B. Hoek, and B. N. Kholodenko. 2007. Ligand-dependent responses of the ErbB signaling network: experimental and modeling analyses. Mol Syst Biol 3:144.
48. Nicolas, F. J., and C. S. Hill. 2003. Attenuation of the TGF-β-Smad signaling pathway in pancreatic tumor cells confers resistance to TGF-β-induced growth arrest. Oncogene 22:3698-3711.
49. Nakao, A., M. Afrakhte, A. Moren, T. Nakayama, J. L. Christian, R. Heuchel, S. Itoh, M. Kawabata, N. E. Heldin, C. H. Heldin, and P. ten Dijke. 1997. Identification of Smad7, a TGFβ-inducible antagonist of TGF-β signalling. Nature 389:631-635.
50. Hayashi, H., S. Abdollah, Y. Qiu, J. Cai, Y. Y. Xu, B. W. Grinnell, M. A. Richardson, J. N. Topper, M. A. Gimbrone, Jr., J. L. Wrana, and D. Falb. 1997. The MAD-related protein Smad7 associates with the TGFβ receptor and functions as an antagonist of TGFβ signaling. Cell 89:1165-1173.
51. He, W., D. C. Dorn, H. Erdjument-Bromage, P. Tempst, M. A. Moore, and J. Massague. 2006. Hematopoiesis controlled by distinct TIF1γ and Smad4 branches of the TGFβ pathway. Cell 125:929-941.
52. Heldin, C. H., and A. Moustakas. 2006. A new twist in Smad signaling. Dev Cell 10:685-686.
53. Levy, L., and C. S. Hill. 2006. Alterations in components of the TGF-β superfamily signaling pathways in human cancer. Cytokine Growth Factor Rev 17:41-58.

54. Bhowmick, N. A., and H. L. Moses. 2005. Tumor-stroma interactions. Curr Opin Genet Dev 15:97-101.
55. Wrzesinski, S. H., Y. Y. Wan, and R. A. Flavell. 2007. Transforming growth factor-beta and the immune response: implications for anticancer therapy. Clin Cancer Res 13:5262-5270.
56. Chen, R. H., R. Ebner, and R. Derynck. 1993. Inactivation of the type II receptor reveals two receptor pathways for the diverse TGF-β activities. Science 260:1335-1338.
57. Geiser, A. G., J. K. Burmester, R. Webbink, A. B. Roberts, and M. B. Sporn. 1992. Inhibition of growth by transforming growth factor-β following fusion of two nonresponsive human carcinoma cell lines. Implication of the type II receptor in growth inhibitory responses. J Biol Chem 267:2588-2593.
58. Feng, X. H., E. H. Filvaroff, and R. Derynck. 1995. Transforming growth factor-β (TGF-β)-induced down-regulation of cyclin A expression requires a functional TGF-beta receptor complex. Characterization of chimeric and truncated type I and type II receptors. J Biol Chem 270:24237-24245.
59. ten Dijke, P., and C. S. Hill. 2004. New insights into TGF-β-Smad signalling. Trends Biochem Sci 29:265-273.
60. Ranganathan, P., A. Agrawal, R. Bhushan, A. K. Chavalmane, R. K. Kalathur, T. Takahashi, and P. Kondaiah. 2007. Expression profiling of genes regulated by TGF-β: differential regulation in normal and tumour cells. BMC Genomics 8:98.

Table Legends

Table 1. Model equations
Table 2. Model parameters

Table 1 Model equations (continued)

Index	Rate equations
1	$v_1 = k_{1a}[TGF\beta][RII] - k_{1d}[TGF\beta : RII]$
2	$v_2 = k_{2a}[TGF\beta : RII][RI] - k_{2d}[R^C]$
3	$v_3 = k_{3\text{int}}[R^C]$
4	$v_4 = k_{4a}[R_{in}^C][S2_{cyt}] - k_{4d}[R_{in}^C : S2_{cyt}]$
5	$v_5 = k_{5cat}[R_{in}^C : S2_{cyt}]$
6	$v_6 = k_{6a}[pS2_{cyt}][S4_{cyt}] - k_{6d}[pS2S4_{cyt}]$
7	$v_7 = k_{7imp}[pS2S4_{cyt}]$
8	$v_8' = k_{8dp}[pS2S4_{nuc}]$
9	$v_9 = k_{9d}[S2S4_{nuc}]$
10	$v_{10} = k_{10imp}[S2_{cyt}] - k_{10\text{exp}}[S2_{nuc}]$
11	$v_{11} = k_{11imp}[S4_{cyt}] - k_{11\text{exp}}[S4_{nuc}]$
12	$v_{12} = k_{12syn} - k_{12\text{deg}}[RII]$
13	$v_{13} = k_{13syn} - k_{13\text{deg}}[RI]$
14	$v_{14} = k_{14syn} - k_{14\text{deg}}[S2_{cyt}]$
15	$v_{15} = k_{15syn} - k_{15\text{deg}}[S4_{cyt}]$
16	$v_{16} = (k_{16\text{deg}} + k_{16lid})[R^C]$
17	$v_{17} = k_{17imp}[pS2_{cyt}]$
18	$v_{18} = k_{18a}[pS2_{nuc}][S4_{nuc}] - k_{18d}[pS2S4_{nuc}]$
19	$v_{19}' = k_{19dp}[pS2_{nuc}]$
20	$v_{20} = k_{20lid}[pS2_{nuc}]$
21	$v_{21} = k_{21\text{int}}[RII] - k_{21rec}[RII_{in}]$
22	$v_{22} = k_{22\text{int}}[RI] - k_{22rec}[RI_{in}]$
23	$v_{23} = k_{23rec}[R_{in}^C]$

Table 1. Model equations

$$\frac{d[RII]}{dt} = -v_1 + v_{12} - v_{21} + v_{23} \qquad \frac{d[TGF\beta : RII]}{dt} = v_1 - v_2$$

$$\frac{d[RI]}{dt} = -v_2 + v_{13} - v_{22} + v_{23} \qquad \frac{d[R^C]}{dt} = v_2 - v_3 - v_{16}$$

$$\frac{d[R_{in}^C]}{dt} = v_3 - v_4 + v_5 - v_{23} \qquad \frac{d[R_{in}^C : S2_{cyt}]}{dt} = v_4 - v_5$$

$$\frac{d[S2_{cyt}]}{dt} = -v_4 - v_{10} + v_{14} \qquad \frac{d[pS2_{cyt}]}{dt} = v_5 - v_6 - v_{17}$$

$$\frac{d[pS2S4_{cyt}]}{dt} = v_6 - v_7 \qquad \frac{d[pS2S4_{nuc}]}{dt} = v_7 - v_8 + v_{18}$$

$$\frac{d[S2S4_{nuc}]}{dt} = v_8 - v_9 \qquad \frac{d[S2_{nuc}]}{dt} = v_9 + v_{10} + v_{19}$$

$$\frac{d[S4_{nuc}]}{dt} = v_9 + v_{11} - v_{18} \qquad \frac{d[S4_{cyt}]}{dt} = -v_6 - v_{11} + v_{15}$$

$$\frac{d[pS2_{nuc}]}{dt} = v_{17} - v_{18} - v_{19} - v_{20} \qquad \frac{d[RII_{in}]}{dt} = v_{21}$$

$$\frac{d[RI_{in}]}{dt} = v_{22}$$

Table 2. Model parameters

parameter	Reaction Step	Value	Unit	Identifiability
k_{1a}	ligand binding	6.60E-03	$molecule^{-1} \cdot min^{-1}$	unidentifiable
k_{1d}	dissociation	2.98E-01	min^{-1}	N/A
k_{2a}	association (RI-RII*)	6.60E-03	$molecule^{-1} \cdot min^{-1}$	unidentifiable
k_{2d}	dissociation	2.98E-01	min^{-1}	N/A
k_{3int}	internalization (R^c)	3.95E-01	min^{-1}	unidentifiable
k_{4a}	association (R^c-S2)	1.50E-04	$molecule^{-1} \cdot min^{-1}$	unidentifiable
k_{4d}	dissociation	9.71E-01	min^{-1}	unidentifiable
k_{5cat}	turnover (pS2)	4.48E+04	min^{-1}	N/A
k_{6a}	association (pS2-S4)	6.00E-03	$molecule^{-1} \cdot min^{-1}$	unidentifiable
k_{6d}	dissociation	1.46E+03	min^{-1}	N/A
k_{7imp}	nuclear import (pS2S4)	8.10E-01	min^{-1}	unidentifiable
k_{8dp}	dephosphorylation (pS2S4)	2.52E-02	min^{-1}	N/A
k_{9d}	dissociation (S2-S4)	1.01E-01	min^{-1}	unidentifiable
k_{10imp}	nuclear import (S2)	1.62E-01	min^{-1}	N/A
k_{10exp}	nuclear export (S2)	3.48E-01	min^{-1}	N/A
k_{11imp}	nuclear import (S4)	2.01E-02	min^{-1}	unidentifiable
k_{11exp}	nuclear export (S4)	1.74E-01	min^{-1}	N/A
k_{12syn}	protein synthesis (RII)	8.00E+00	$molecule \cdot min^{-1} \cdot cell^{-1}$	N/A
k_{12deg}	degradation (RII)	2.80E-02	min^{-1}	N/A
k_{13syn}	protein synthesis (RI)	8.00E+00	$molecule \cdot min^{-1} \cdot cell^{-1}$	N/A
k_{13deg}	degradation (RI)	2.80E-02	min^{-1}	N/A
k_{14syn}	protein synthesis (S2)	2.74E+01	$molecule \cdot min^{-1} \cdot cell^{-1}$	N/A
k_{14deg}	degradation (S2)	6.46E-04	min^{-1}	N/A
k_{15syn}	protein synthesis (S4)	5.00E+01	$molecule \cdot min^{-1} \cdot cell^{-1}$	N/A
k_{15deg}	degradation (S4)	1.20E-03	min^{-1}	N/A
k_{16deg}	constitutive deg (R^c)	2.80E-02	min^{-1}	N/A
k_{16lid}	ligand-induced deg (R^c)	3.95E-01	min^{-1}	N/A
k_{17imp}	nuclear import (pS2)	5.03E-01	min^{-1}	identifiable
k_{18a}	association (pS2-S4)	1.67E-04	$molecule^{-1} \cdot min^{-1}$	unidentifiable
k_{18d}	dissociation	9.09E-01	min^{-1}	unidentifiable
k_{19dp}	dephosphorylation (pS2)	2.52E-02	min^{-1}	N/A
k_{20lid}	ligand-induced deg (pS2)	5.40E-03	min^{-1}	identifiable
k_{21int}	internalization (RII)	3.95E-01	min^{-1}	N/A
k_{21rec}	recycling (RII)	3.95E-02	min^{-1}	N/A
k_{22int}	internalization (RI)	3.95E-01	min^{-1}	N/A
k_{22rec}	recycling (RI)	3.95E-02	min^{-1}	N/A
k_{23rec}	recycling (R^c)	3.95E-02	min^{-1}	N/A

Figure Legends

Figure 1. Schematic representation of the pathway components in the integrated model. Numbers in the cartoon refer to the chemical reaction indices in Table 1.

Figure 2. Model fit to experimental data: (A) total phosphorylated Smad2 in the nucleus [17], (B) total phosphorylated Smad2 in the cytoplasm [27], (C) total nuclear Smad2 [26], (D) total cytoplasmic Smad2 [27], and (E) total nuclear Smad4 [27] in response to TGF-β stimulation.

Figure 3. Model validation: (A) total cellular pSamd2 [40]; (B) ratio of cellular pSmad2 to total Smad2 in response to the step input of TGF-β [38]; (C) ratio of cellular pSmad2 to total Smad2 in response to the pulse input of TGF-β [38]; (D) total cytoplasmic Smad4 [27].

Figure 4. Model parameter sensitivities for select parameters with the greatest influence on phosphorylated Smad2-Smad4 complex in the nucleus. Parameters with maximum normalized sensitivity coefficients exceeding 0.5 in absolute value at any point in time are shown.

Figure 5. The effect of blocking translocation of monomeric pSmad2 (red) or heteromeric pSmad2 (blue)

Figure 6. The effect of variations in the rate of Smad2 phosphorylation (A), nuclear pSmad2-Smad4 association (B), pSmad2 degradation (C), nuclear pSmad2 dephosphorylation (D), and nuclear import of pSmad2 (E) on the dynamics of nuclear pSmad2-Smad4 complex. Each indicated parameter value was increased (blue) or decreased (red) 10 fold.

Figure 7. The effect of different concentrations of TGF-β on the dynamic responses of internalized activated receptor complex (A) and activated Smad2-Smad4 complex in the nucleus (B) under normal conditions, and internalized activated receptor complex (C), and activated Smad2-Smad4 complex in the nucleus (D) under cancerous conditions with 10-fold reduction in initial levels and protein synthesis rate constants of both Type I and Type II receptors.

Figure 8. *In silico* mutation results: Responses of internalized activated receptor complex (A) and nuclear pSmad-Smad4 complex (B) to 10-fold reduction in initial levels and protein synthesis rate constants of both Type I and Type II receptors. (C) Temporal profiles of phosphorylated Smad2 in HaCaT cells (red, from Lo and Massague [40]), LNCaP cells (blue, our experiments) and C4-2 cells (green, our experiments) in response to 200pM (for A) or 400pM (for B and C) of TGF-β. All data points were normalized with respect to the maximum intensity value of pSmad2 of each profile.

Figure 9. Model predictions for nuclear Smad4 (A) and nuclear pSmad2-Smad4 complex (B) upon TGF-β stimulation (80pM) under cancerous conditions; 10-fold reduction in the initial levels and the protein synthesis rate constants of both Type I and Type II, and 10-

fold increase in rates of degradation of either Smad4 (A: red; B: green) or pSmad2 (B, blue) or both (B, red).

Figure 10. Alternative TGF-β-induced responses determined by nuclear pSmad2-binding partners. While Smad4 forms transcriptional complexes with receptor-phosphorylated Smad2/3 and mediates antiproliferative responses, TIF1γ specifically recognizes receptor-activated Smad2/3 and mediates differentiation of hematopoietic stem/progenitor cells. (Adapted from He *et al.* [51])

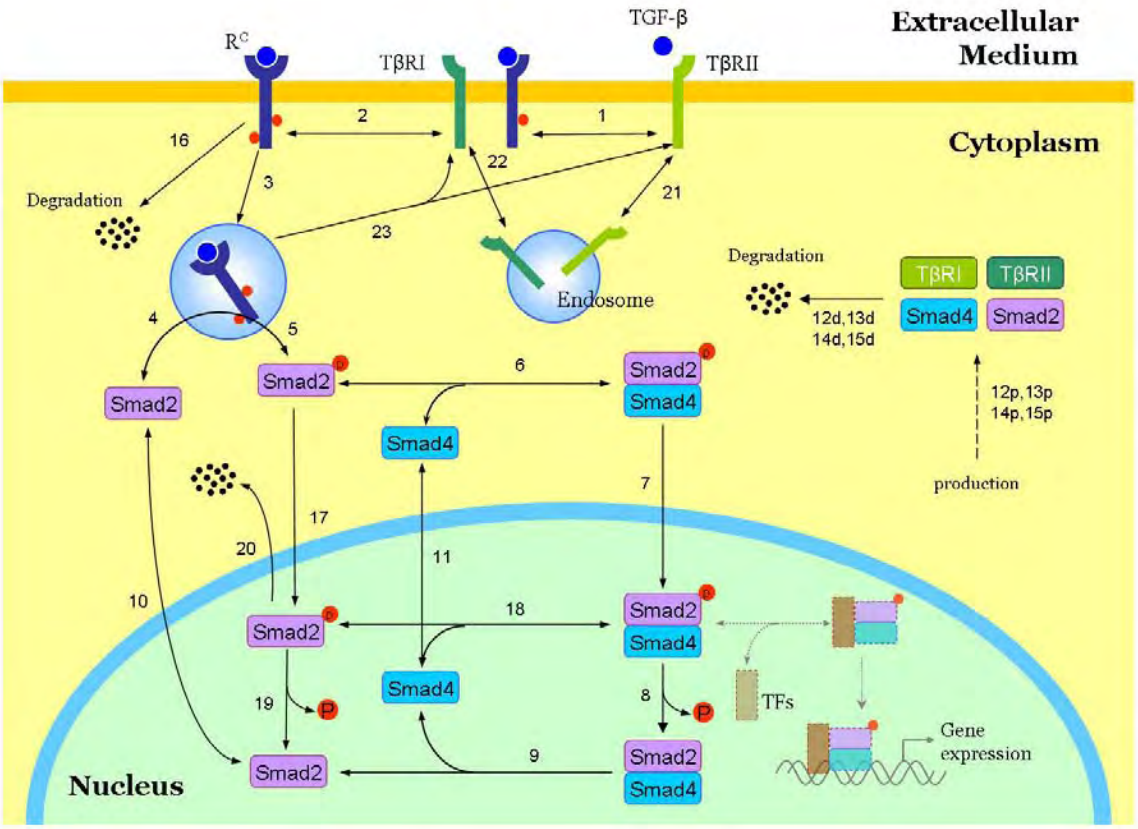
Extracellular Medium
Cytoplasm
Nucleus
TGF-β
TβRI
TβRII
Endosome
Degradation
Smad2
Smad4
TFs
Gene expression
production
12d,13d
14d,15d
12p,13p
14p,15p

Figure 1

Figure 2A.

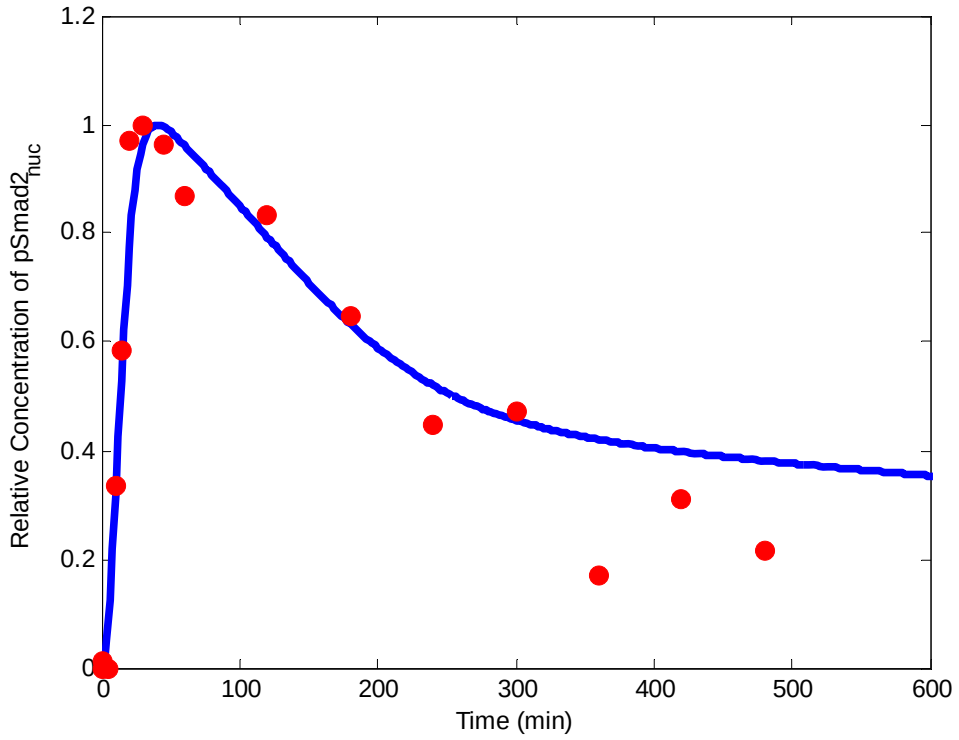
Relative Concentration of pSmad2nuc
Time (min)
0
0.2
0.4
0.6
0.8
1
1.2
0
100
200
300
400
500
600

2B.

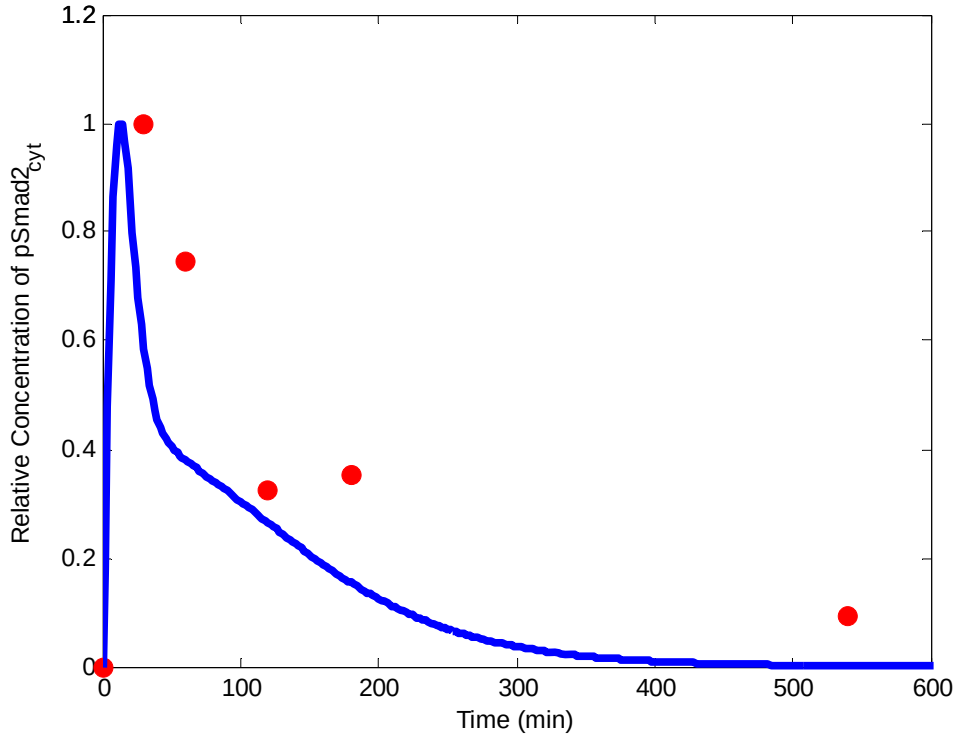
Relative Concentration of pSmad2cyt
Time (min)
0
0.2
0.4
0.6
0.8
1
1.2
0
100
200
300
400
500
600

2C.

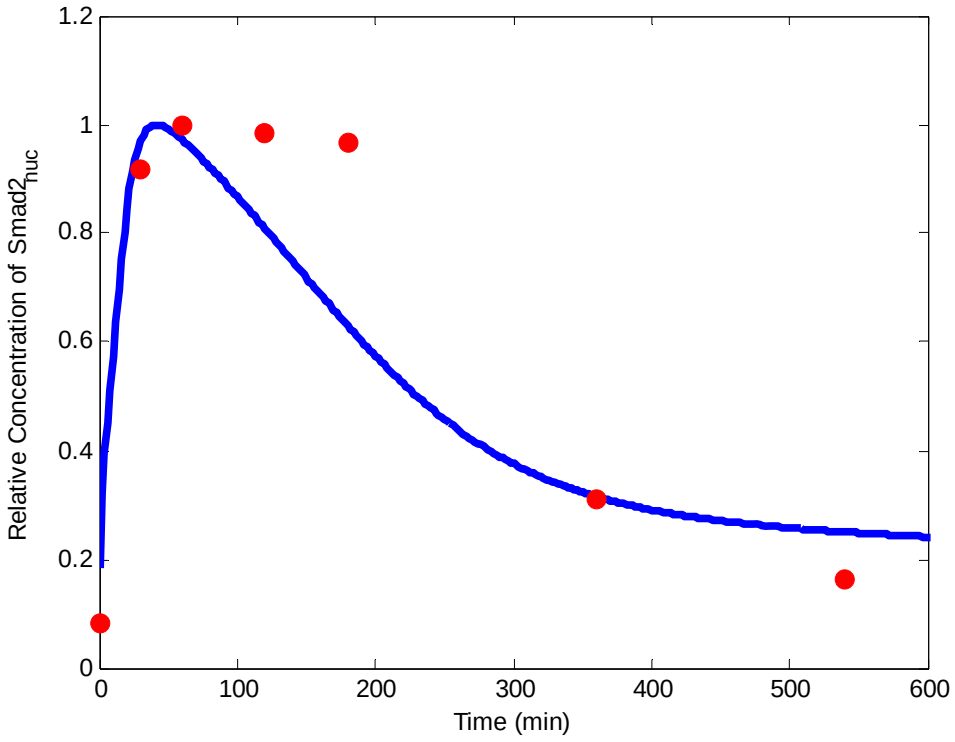
Relative Concentration of Smad2nuc
Time (min)
0
0.2
0.4
0.6
0.8
1
1.2
0
100
200
300
400
500
600

2D.

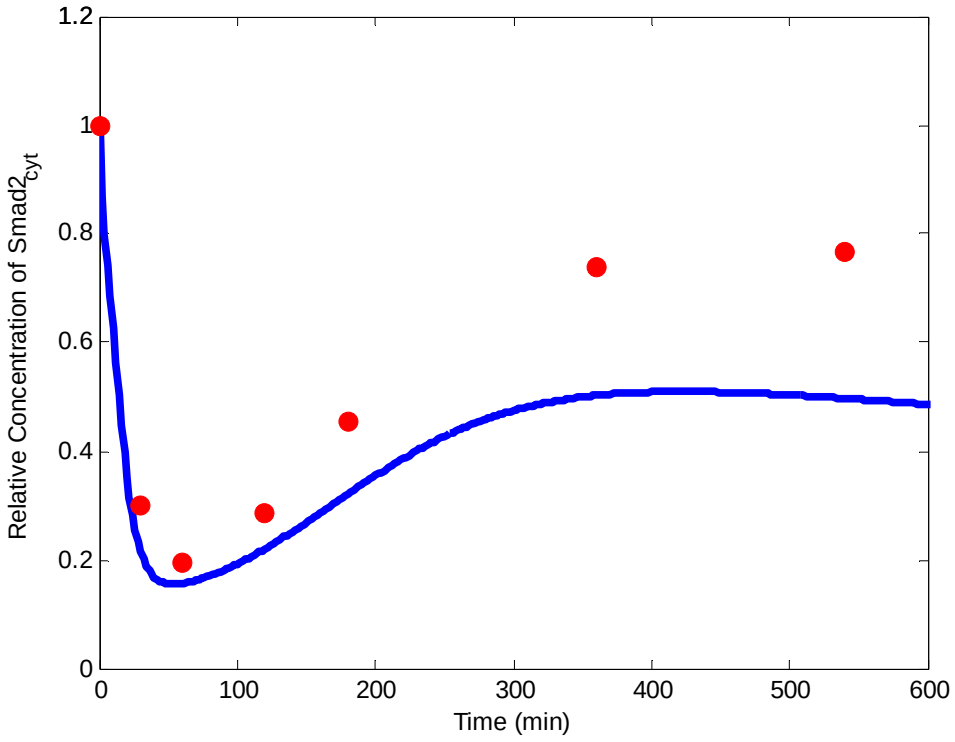
Relative Concentration of Smad2cyt
Time (min)
0
0.2
0.4
0.6
0.8
1
1.2
0
100
200
300
400
500
600

2E.

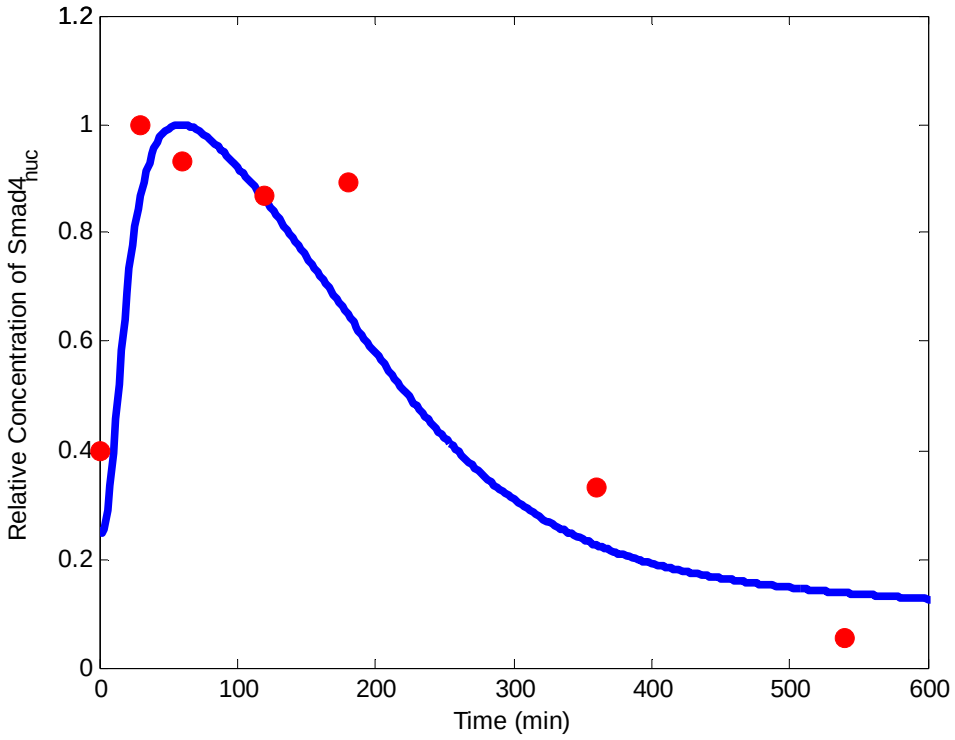
1.2
1
0.8
0.6
0.4
0.2
0
Relative Concentration of Smad4huc
0
100
200
300
400
500
600
Time (min)

Figure 2

Figure 3A.

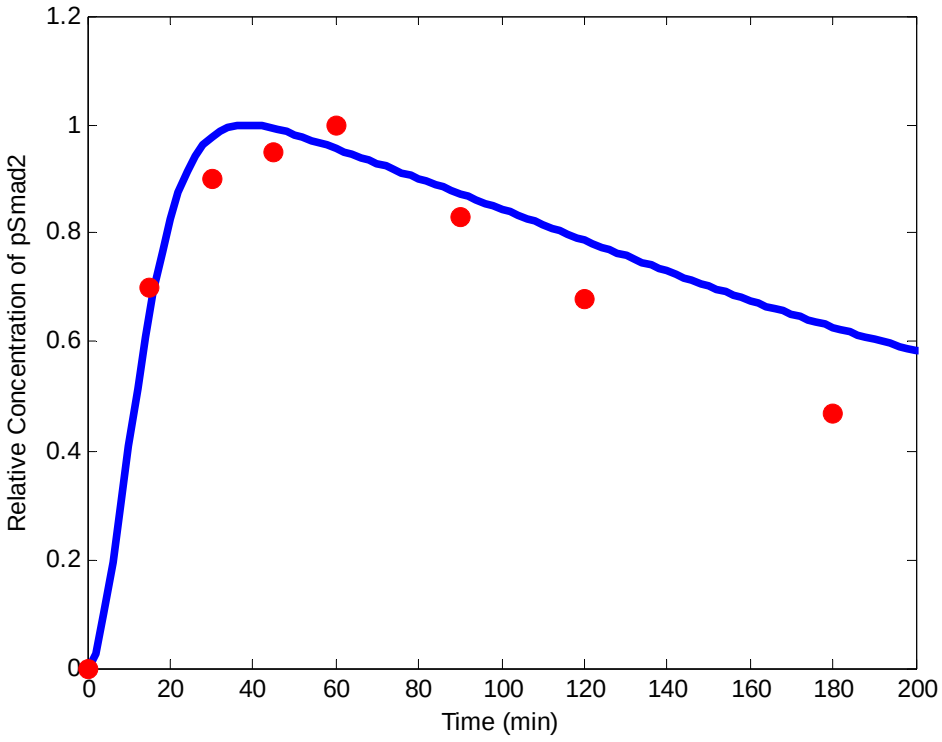
Relative Concentration of pSmad2
Time (min)
0
0.2
0.4
0.6
0.8
1
1.2
0
20
40
60
80
100
120
140
160
180
200

3B.

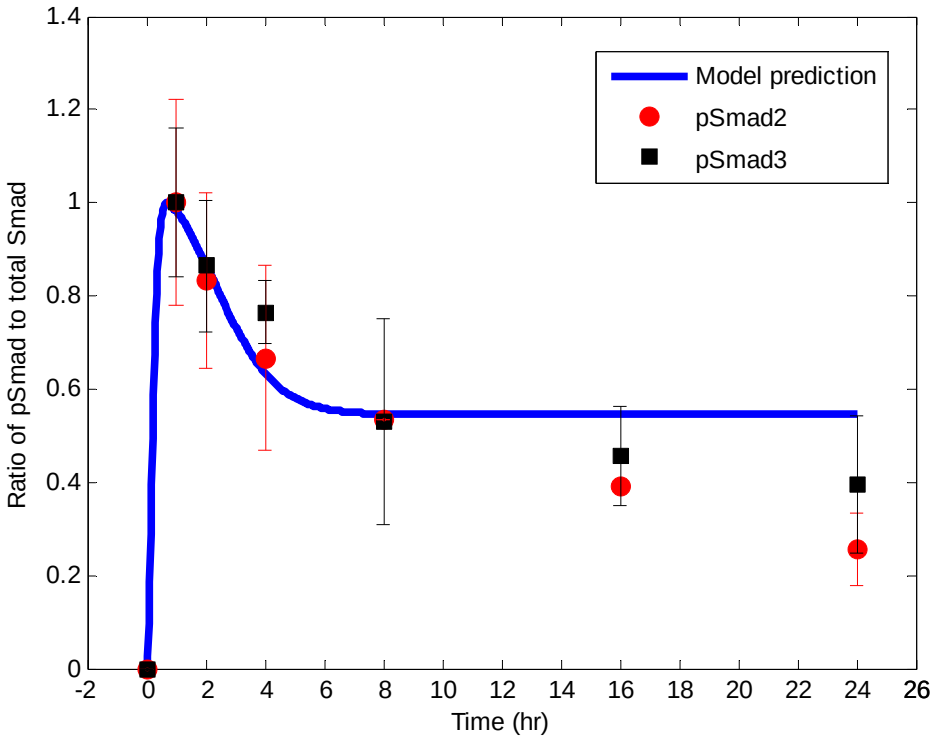
Model prediction
pSmad2
pSmad3
Ratio of pSmad to total Smad
Time (hr)
0
0.2
0.4
0.6
0.8
1
1.2
1.4
-2
0
2
4
6
8
10
12
14
16
18
20
22
24
26

3C.

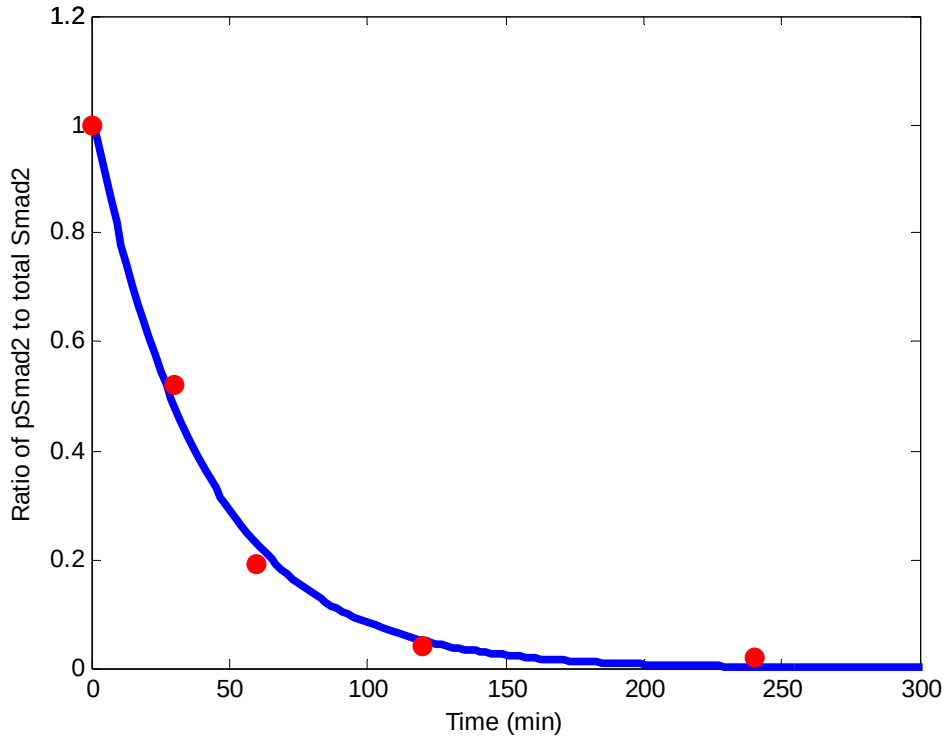

3D.

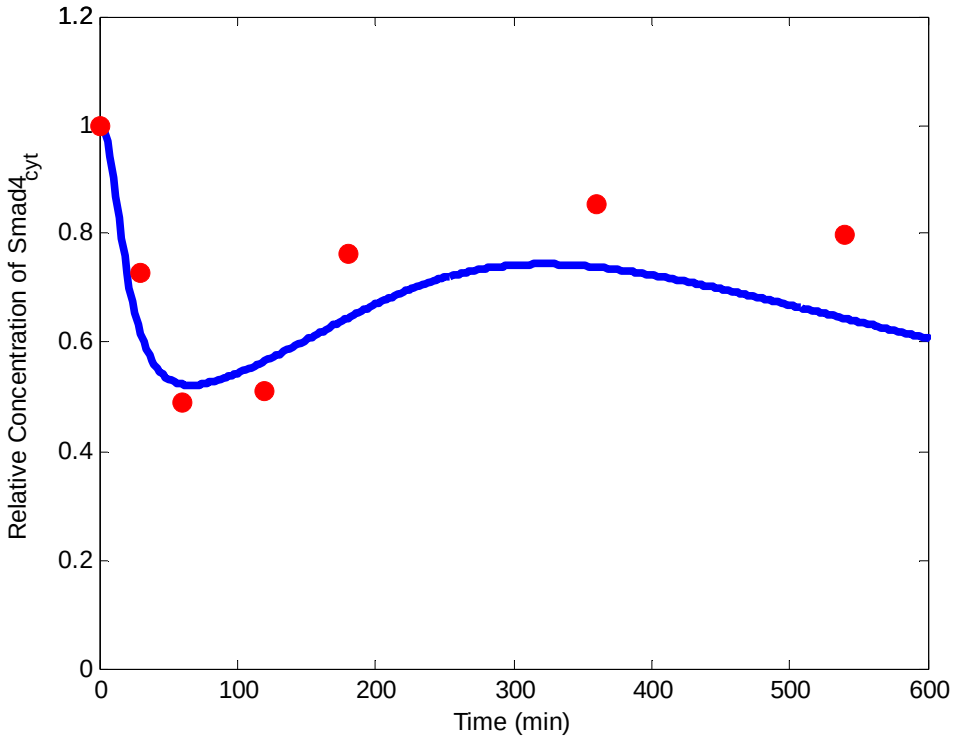

Figure 3

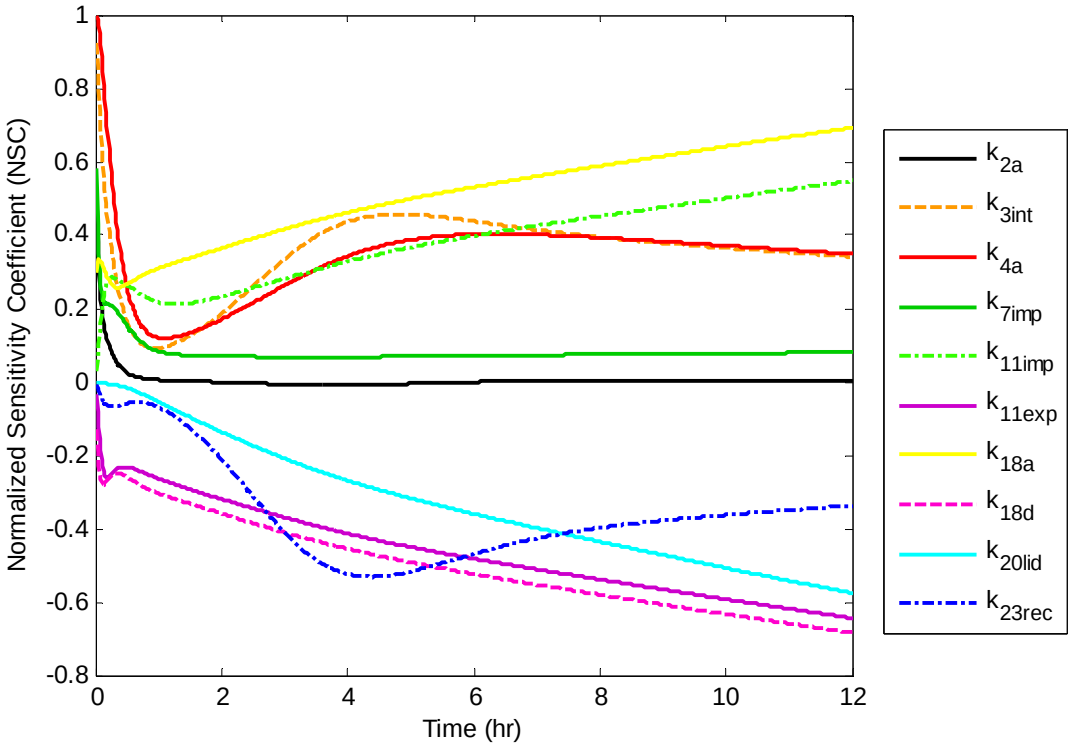
Normalized Sensitivity Coefficient (NSC)
Time (hr)
1
0.8
0.6
0.4
0.2
0
-0.2
-0.4
-0.6
-0.8
0
2
4
6
8
10
12
k2a
k3int
k4a
k7imp
k11imp
k11exp
k18a
k18d
k20lid
k23rec

Figure 4

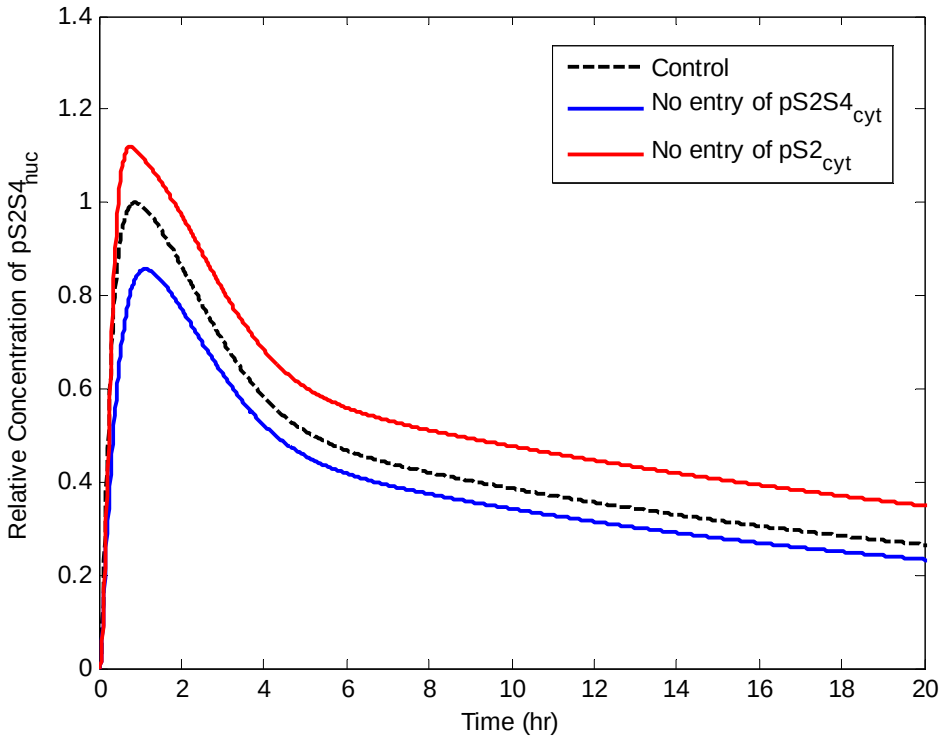
Control
No entry of pS2S4cyt
No entry of pS2cyt
Relative Concentration of pS2S4nuc
Time (hr)
0
0.2
0.4
0.6
0.8
1
1.2
1.4
0
2
4
6
8
10
12
14
16
18
20

Figure 5

Figure 6A.

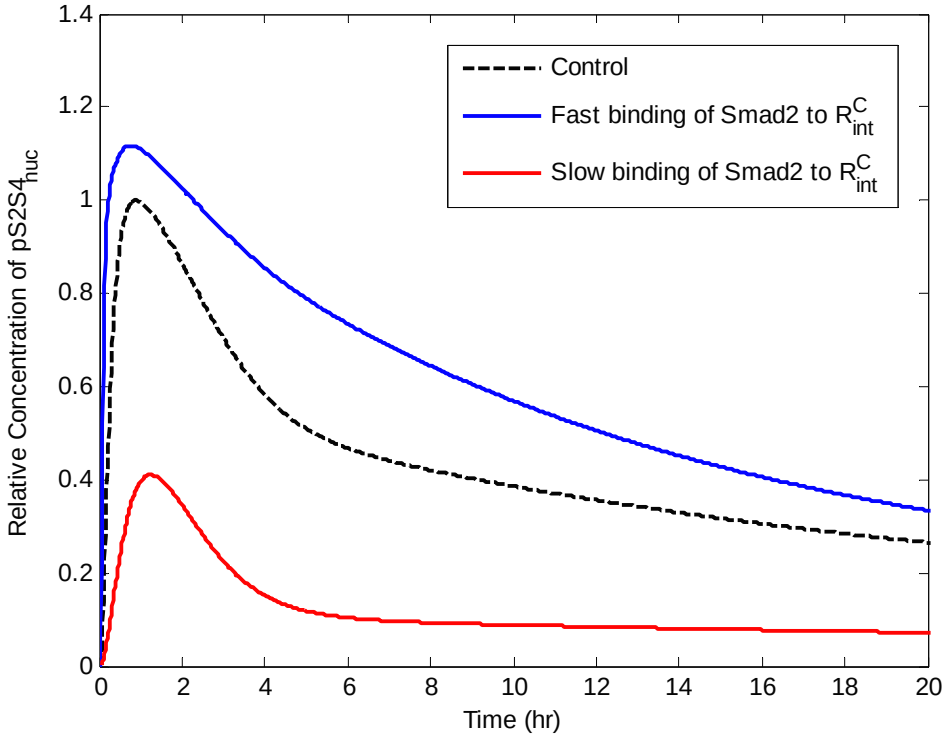
Control
Fast binding of Smad2 to R_{int}^{C}
Slow binding of Smad2 to R_{int}^{C}
Relative Concentration of $pS2S4_{huc}$
Time (hr)
0
0.2
0.4
0.6
0.8
1
1.2
1.4
0
2
4
6
8
10
12
14
16
18
20

6B.

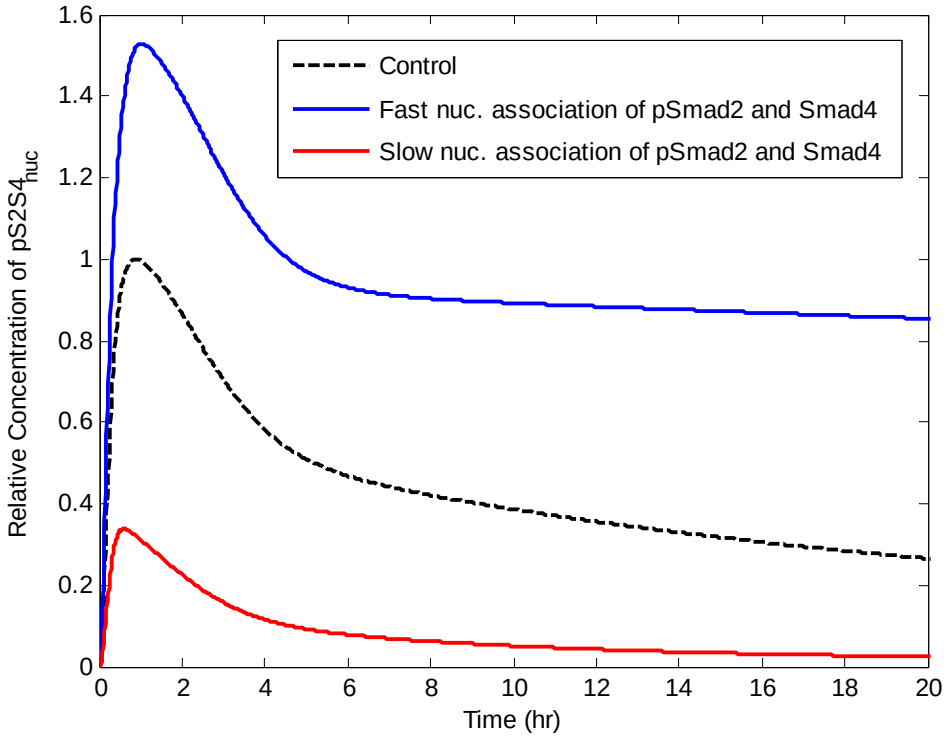
Control
Fast nuc. association of pSmad2 and Smad4
Slow nuc. association of pSmad2 and Smad4
Relative Concentration of $pS2S4_{huc}$
Time (hr)
0
0.2
0.4
0.6
0.8
1
1.2
1.4
1.6
0
2
4
6
8
10
12
14
16
18
20

6C.

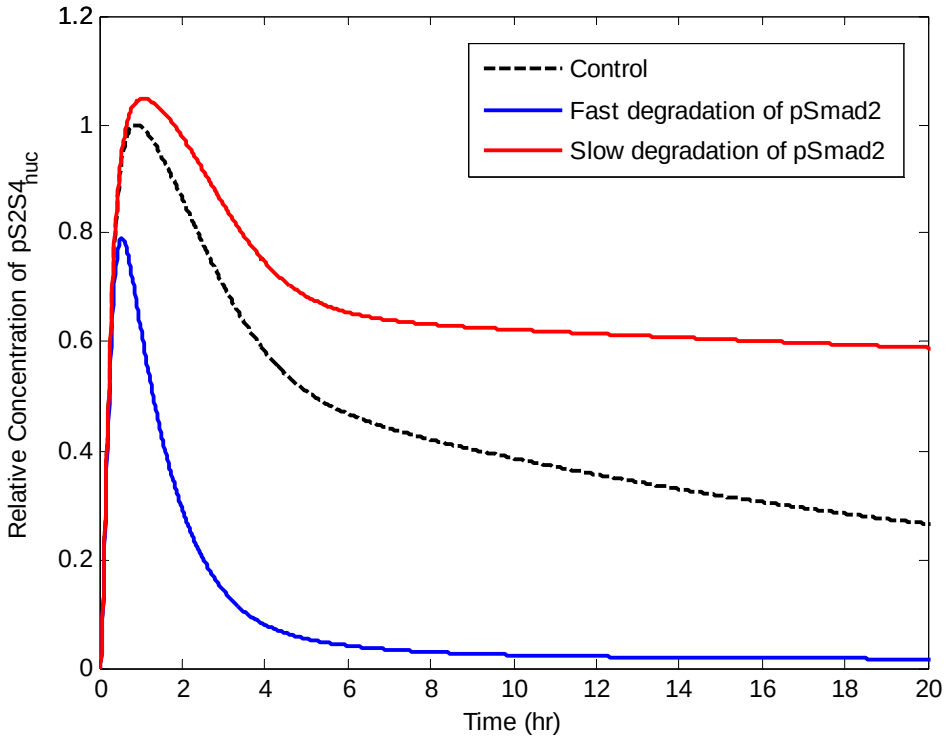
Control
Fast degradation of pSmad2
Slow degradation of pSmad2
Relative Concentration of pS2S4huc
Time (hr)
0
0.2
0.4
0.6
0.8
1
1.2
0
2
4
6
8
10
12
14
16
18
20

6D.

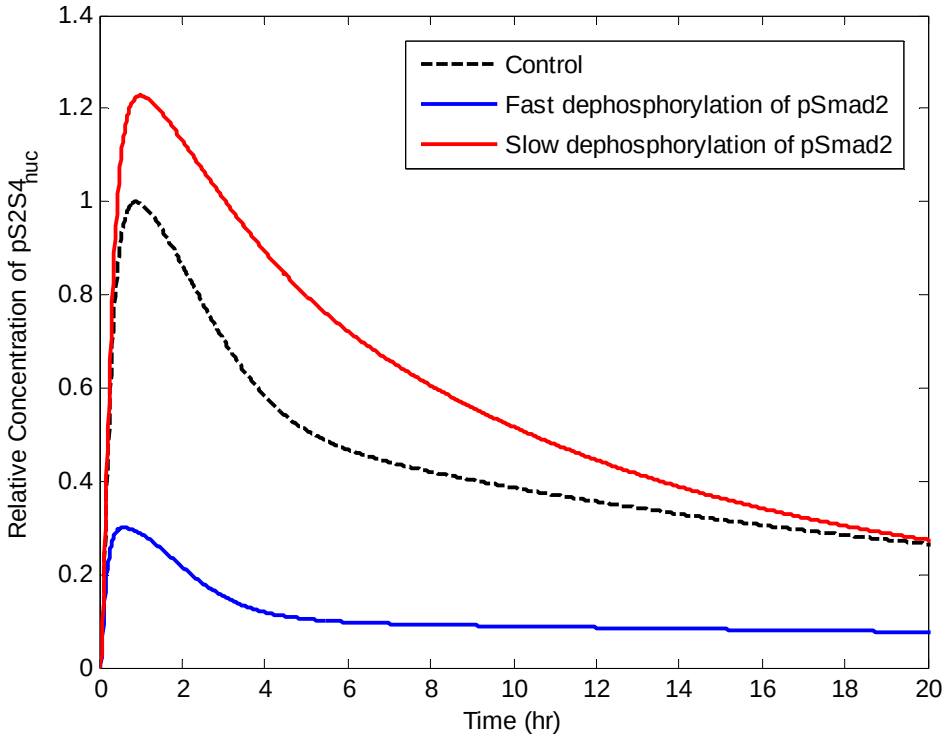
Control
Fast dephosphorylation of pSmad2
Slow dephosphorylation of pSmad2
Relative Concentration of pS2S4huc
Time (hr)
0
0.2
0.4
0.6
0.8
1
1.2
1.4
0
2
4
6
8
10
12
14
16
18
20

6E.

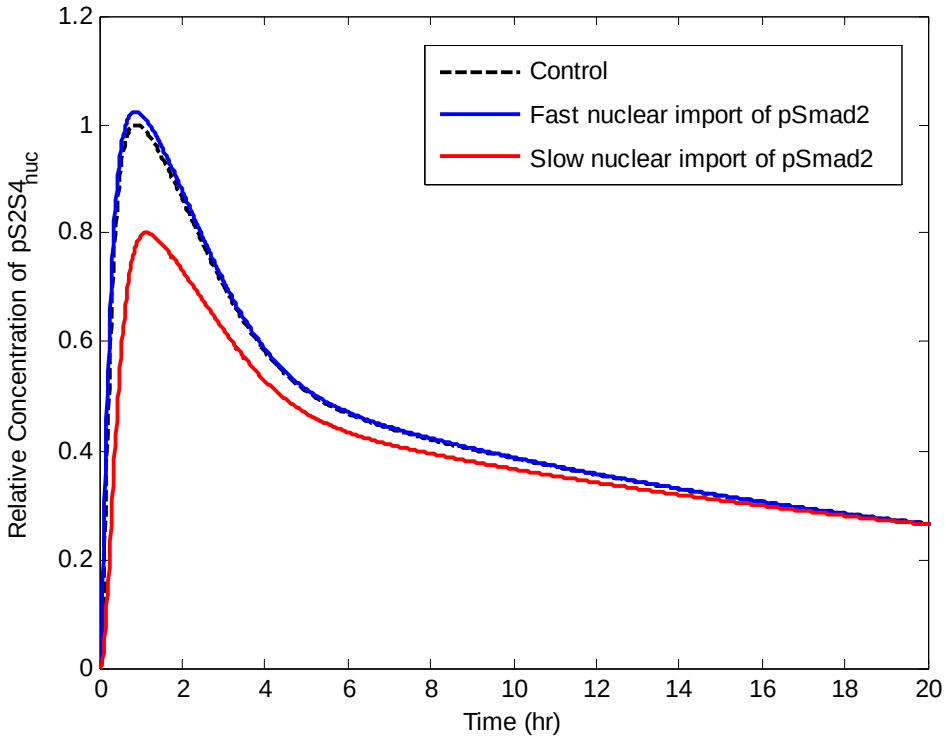
Control
Fast nuclear import of pSmad2
Slow nuclear import of pSmad2
Relative Concentration of pS2S4nuc
Time (hr)
0
0.2
0.4
0.6
0.8
1
1.2
0
2
4
6
8
10
12
14
16
18
20

Figure 6

Figure 7A & 7B

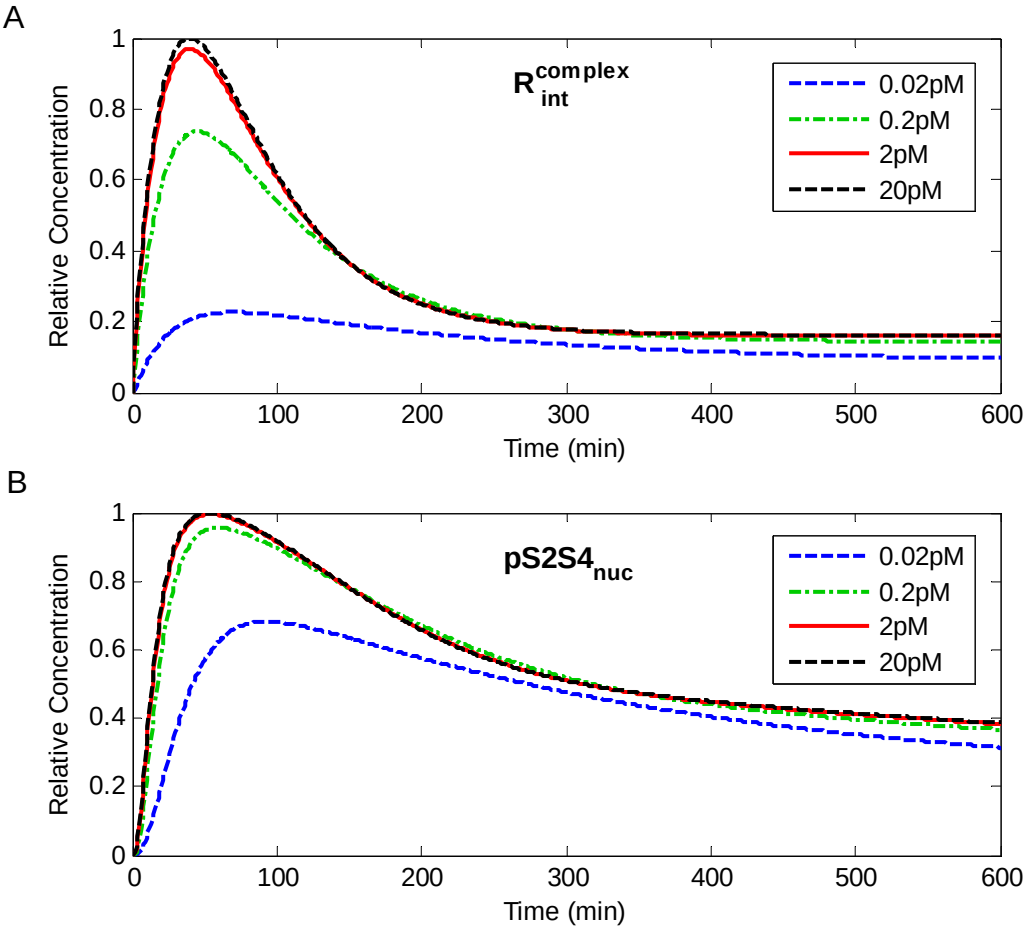
A
$R^{complex}_{int}$
0.02pM
0.2pM
2pM
20pM
Relative Concentration
Time (min)
B
$pS2S4_{nuc}$
0.02pM
0.2pM
2pM
20pM
Relative Concentration
Time (min)

Figure 7C & 7D

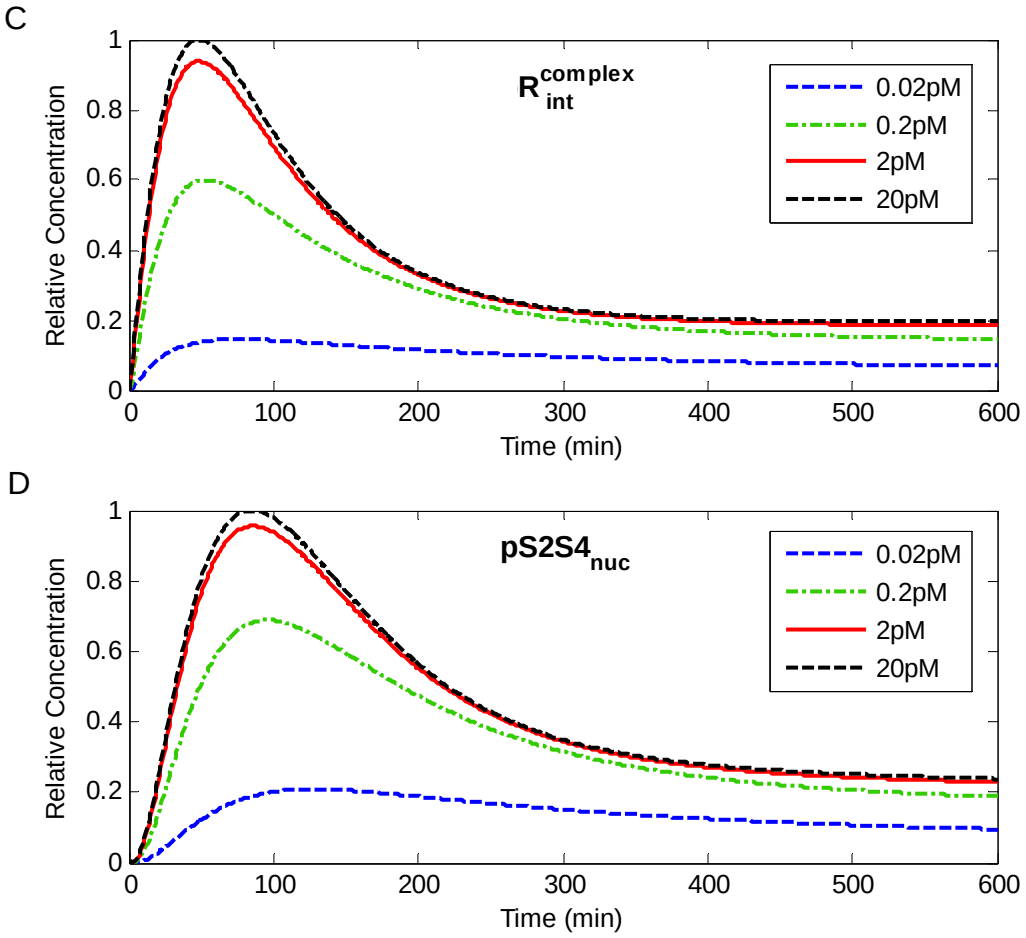

Figure 7

Figure 8A.

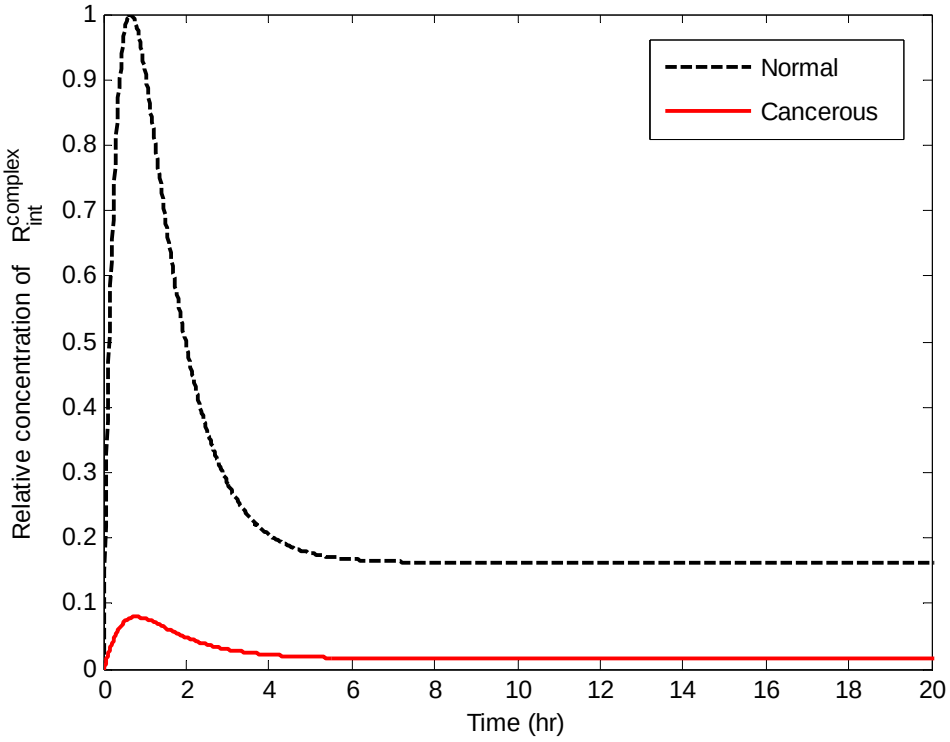
Normal
Cancerous
Relative concentration of $R_{int}^{complex}$
Time (hr)
0
0.1
0.2
0.3
0.4
0.5
0.6
0.7
0.8
0.9
1
0
2
4
6
8
10
12
14
16
18
20

8B.

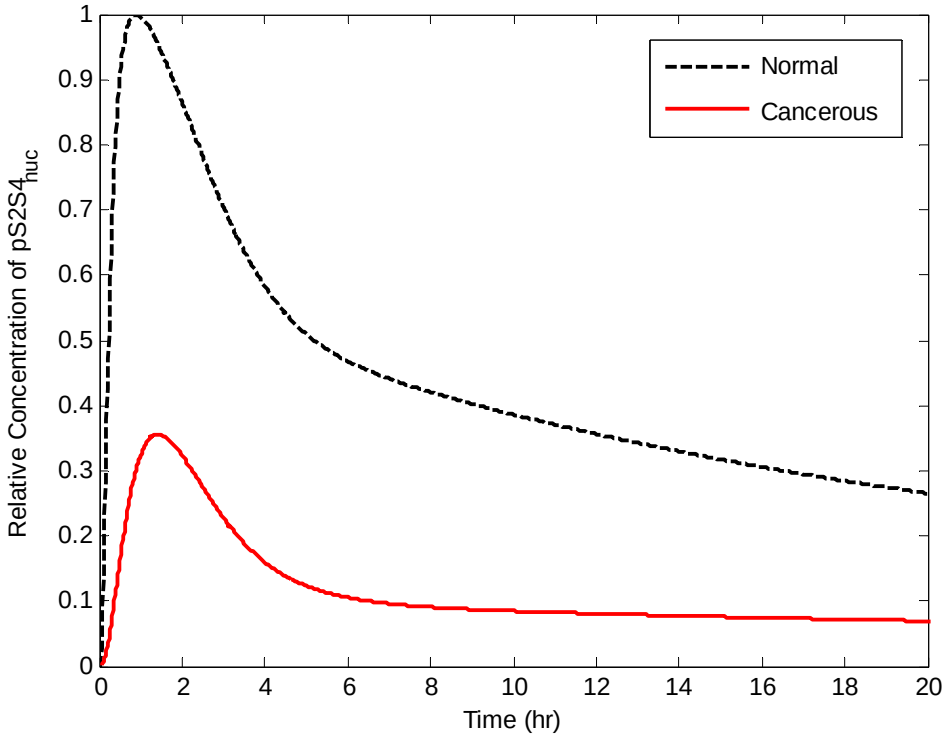
Normal
Cancerous
Relative Concentration of $pS2S4_{huc}$
Time (hr)
0
0.1
0.2
0.3
0.4
0.5
0.6
0.7
0.8
0.9
1
0
2
4
6
8
10
12
14
16
18
20

8C.

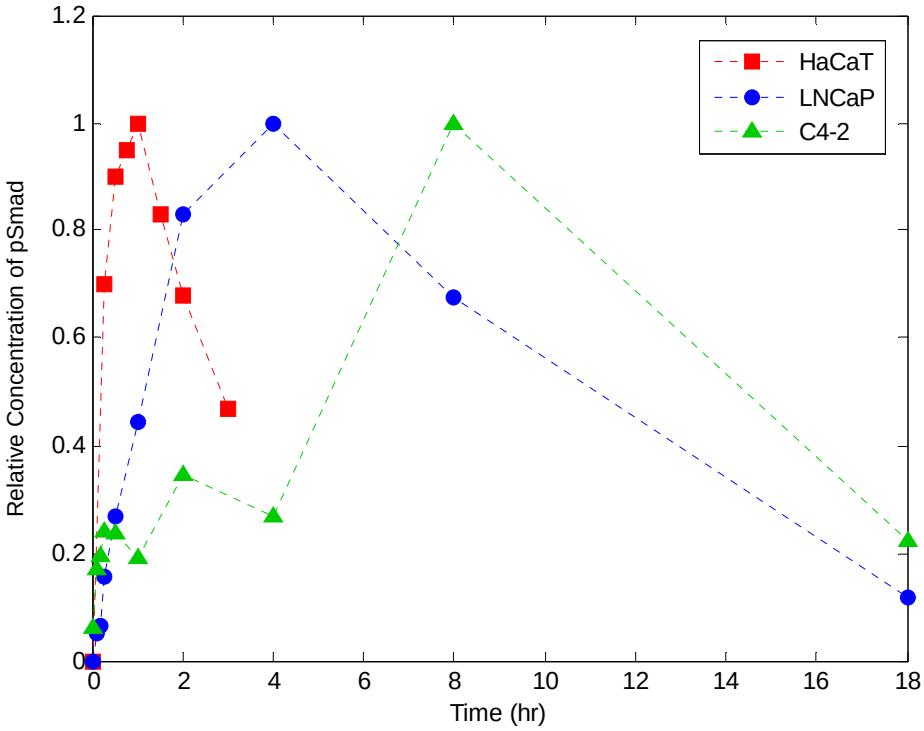
HaCaT
LNCaP
C4-2
Relative Concentration of pSmad
Time (hr)
0
0.2
0.4
0.6
0.8
1
1.2
0
2
4
6
8
10
12
14
16
18

Figure 8

9A

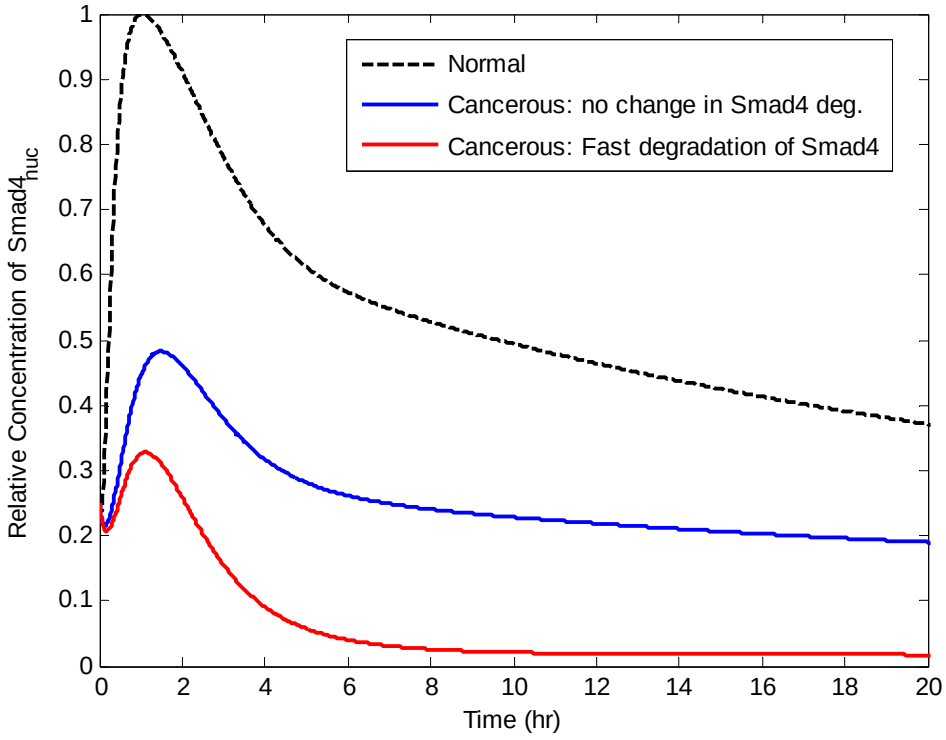

9B

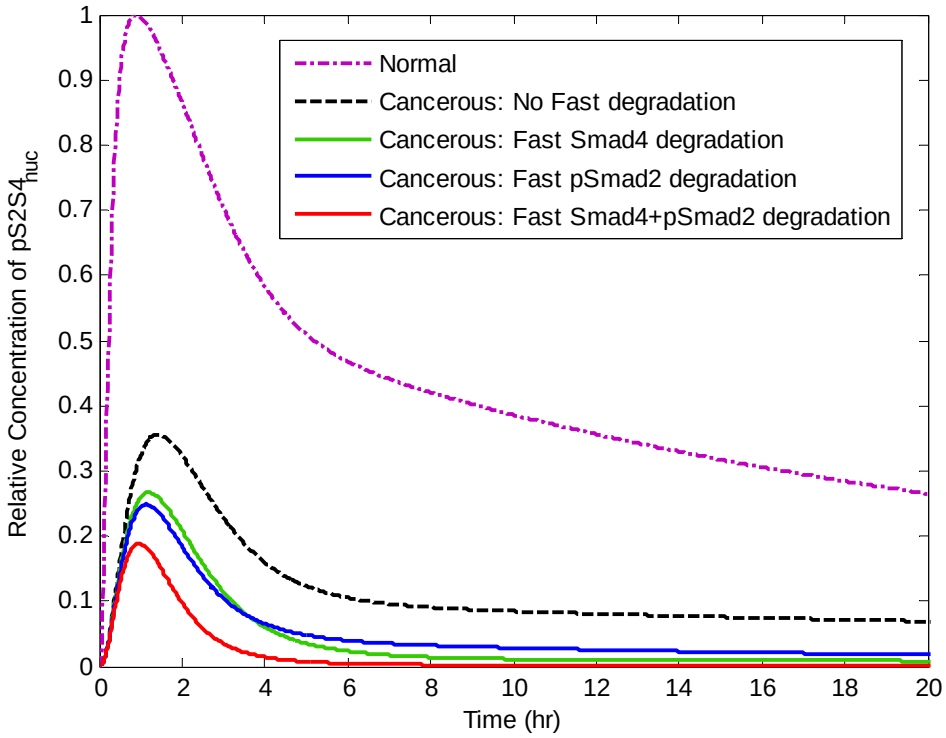

Figure 9

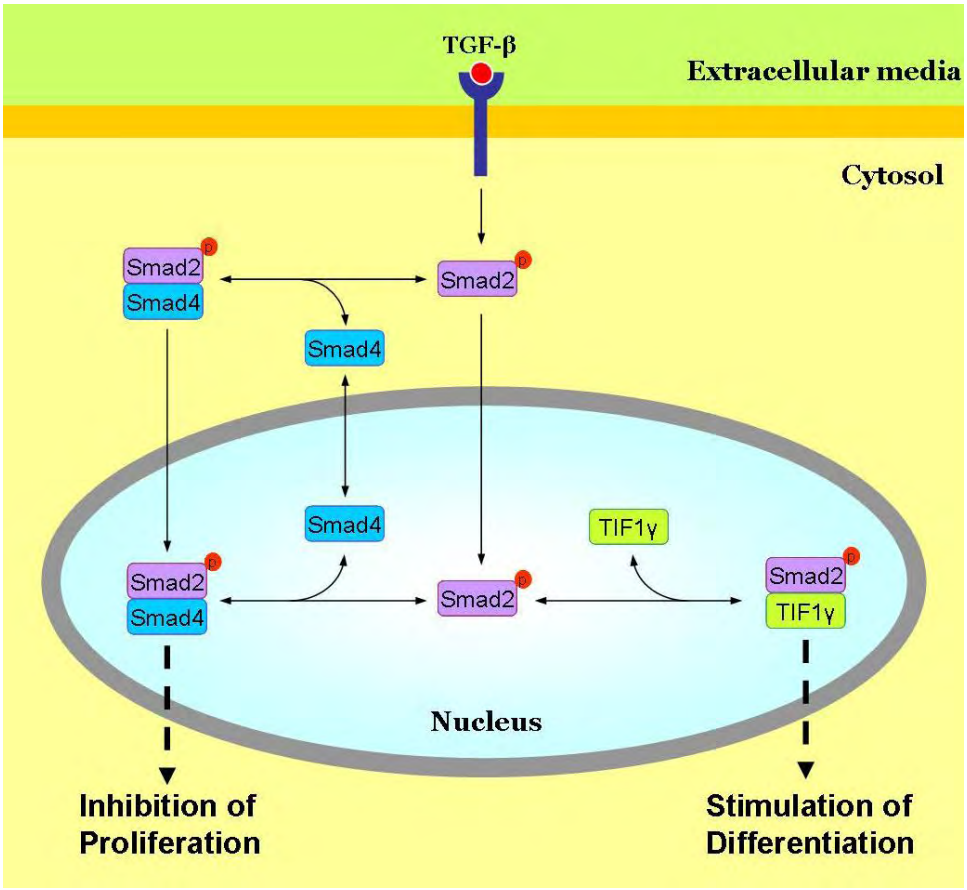
TGF-β
Extracellular media
Cytosol
Smad2
Smad4
Smad2
Smad4
Smad4
Smad4
TIF1γ
Smad2
Smad4
Smad2
Smad2
TIF1γ
Nucleus
Inhibition of
Proliferation
Stimulation of
Differentiation

Figure 10